Academic Year 2019-2020

Faculty Pharmaceutical, Biomedical and Veterinary Sciences

Biomedical Sciences

Collicular-driven stopping behavior is modulated by the posterior paralaminar nuclei of the thalamus

By:

Dani Lemmon

Master Thesis in partial fulfillment of the requirements for the degree

Master in Biomedical Sciences

Promoter: Dr. Karl Farrow

Copromoter: Prof. Dr. Annemie Van Der Linden

Coach: Arnau Sans-Dublanc

Neuro-electronics Research Flanders (NERF)

Kapeldreef 75

3000 Leuven

Belgium

Acknowledgments

My Master's internship in the Farrow Lab at NERF has been an extremely positive and empowering experience, and I want to give a specific thank you to all those who made it so. The Farrow Lab is one of a kind!

To Karl Farrow, thanks for being a fantastic promoter! I am so appreciative of your constant support, mentorship, philosophical answers to life's queries, and nearly instantaneous email replies. Thank you for investing time and lab resources toward my scientific progression.

To Arnau, a huge thank you for your mentorship. Thanks for your unfailing patience and attention to the details in training me to perform viral injections, fiber implantations, perfusions, opto tests... and the list goes on. Thank you for the constructive feedback and for the healthy dose of sarcasm throughout the year. It has been especially rewarding to be involved in the opto-fUSi project and publication this year. Thank you to you and Ania for making my contribution to Figure 8 of the paper a reality!

To Ania, my coding confidant, thank you for your immense help in getting started with my analysis in Python, for sharing in the joy of successful debugging, and for your encouragement to push through the grind. Every time I use .groupby(), I thank my lucky stars that you pointed it out to me on day 1!

A hearty thank you to the other members of the Farrow lab (Katja, Norma, Chen, Joana, Bram, Subhash) for the good company in and outside of the lab. Thanks for your friendship, sharing laughs over lunch & coffee, and answering many frantic questions from a novice experimenter!

Thanks to my fellow master's students (Firdaouss, Daan, Laure, Soraya, Benjamin) for your friendship, empathy, and for all the good memories I have from the months we were in the lab together.

A special thank you to NERF, Imec, and University of Antwerp for allowing the organization of this internship and to the Flemish government for supporting my studies with a Master Mind scholarship. Thank you to my co-readers for your willingness to read and evaluate my work and to Annemie Van Der Linden for the support as my internal co-promoter.

To Braxton, thanks for saving the day when my hard drive failed just as I started analysis and reviving your battery-less 2010 Macbook Pro with Ubuntu, Anaconda, Inkscape, and Fiji installations as a bonus!

Corona measures impact statement

Due to the exceptional circumstances brought about by the coronavirus pandemic, I have been asked to add a section defining how the corona measures affected my master's internship project and thesis.

Imec in Leuven, the location of my external internship, was early to implement safety measures and consequently allowed some onsite work to continue through the duration of the lockdown period. The Imec prevention team enacted strict distancing guidelines, active disinfection of equipment and space, and personal protective equipment to minimize risks. After deliberation with my promoter in Leuven and co-promoter in Antwerp, we determined I could safely continue my activity in the lab to finish the experiments I had started prior to the lockdown. This decision was based on the guidelines from the government, University of Antwerp, Imec, and NERF. I was, however, unable to begin new experiments; consequently, my retrograde viral tracing experiment includes only one animal.

Following completion of my practical work in May, I performed all analysis and writing from home due to capacity restrictions in the office spaces at Imec. During this period, I had daily support from my promoter and mentor. We communicated frequently via email and held virtual meetings regularly on Microsoft Teams.

In summary, I was very fortunate to be able to complete my data collection in the lab and to have a very good support system during the analysis and writing period at home. As such, my thesis and the definition of the assignment were not impacted heavily by the corona measures.

Table of Contents

Abstract

Innate responses to relevant stimuli are critical to animal survival; however, the complex circuitry underlying these behaviors is not well-defined. The superior colliculus of the mammalian midbrain plays a key role in mediating visually guided behaviors by integrating sensory input to induce eye, head and body movements towards or away from appetitive or threatening stimuli. The genetically-identified cell-types in the superior colliculus of the mouse have been shown to play a role in specific defensive behaviors, such as freezing behavior induced by activation of collicular cells expressing PV or CAMKII. Recently, activation of NTSR neurons in the colliculus was shown to induce stopping behavior. Whole brain functional recording during optogenetic stimulation of NTSR collicular neurons revealed the posterior paralaminar nuclei of the thalamus (PPnT) as a potential player in collicular-driven behaviors. Here we examine the contribution of the PPnT to NTSR collicular-driven stopping behavior. We show that chemogenetic inhibition of the PPnT facilitates habituation to stimulation of NTSR collicular neurons, resulting in attenuation of stopping behavior. We also provide suggestive evidence for inputs to the PPnT in mice using retrograde viral tracing. Our results suggest that the PPnT prevents behavioral adaptation to repeated presentation of a stimulus, uncovering a novel role for the PPnT in collicular-driven innate behaviors.

List of abbreviations

AAV	adeno-associated virus
AMd	anteromedial nucleus of thalamus, dorsal part
AMG	amygdala
AMv	anteromedial nucleus of thalamus, ventral part
AP	anterior-posterior
AUD	auditory area
AUDp	auditory area, posterior
AUDv	auditory area, ventral
CAMKII	calmodulin-dependent protein kinase II
CeA	central nucleus, amygdala
ChR2	channelrhodopsin-2
CM	central medial nucleus of thalamus
CNO	clozapine-N-oxide
CPu	caudoputamen
CTRL	control
CUN	cuneiform nucleus
DAPI	4’,6-diamidino-2-phenylindole
DG	dentate gyrus
DIO	double-floxed inverse open reading frame
dlPAG	dorsolateral periaqueductal gray
dPAG	dorsal periaqueductal gray
DPSS	diode-pumped solid-state (laser)
DREADDs	Designer Receptors Exclusively Activated by Designer Drugs
dSC	deep layers of superior colliculus
DV	dorsal-ventral
ECT	ectorhinal cortex
EFYP	enhanced yellow fluorescent protein
fMRI	functional magentic resonance imaging
fps	frames per second
fUSi	functional ultrasound imaging
GAD2	glutamate decarboxylase 2
GFP	green flourescent protein
hEF1	human enhancer of filamentation 1
HIPP	hippocampus
hM4D(Gi)	human Gi-coupled M4 muscarinic receptor
HSV	herpes simplex virus

hSyn	human synapsin
HY	hypothalamus
i.p.	intraperitonial
IAM	interoanteromedial nucleus of thalamus
IC	inferior colliculus
IQR	inter-quartile range
LA	lateral amygdalar complex
LED	light-emitting diode
LGN	lateral geniculate nucleus of thalamus
LGNd	lateral geniculate nucleus, dorsal part
LGNv	lateral geniculate nucleus, ventral part
LP	lateral posterior nucleus of thalamus
MAD	mean absolute deviation
MeA	medial nucleus, amygdala
MGm	medial geniculate complex, medial division
ML	medial-lateral
NTSR	neurotensin receptor
PAG	periaqueductal gray
PB	parabrachial nucleus
PBG	parabigeminal nucleus
PBS	phosphate-buffered saline
PFA	paraformaldehyde
PG	pontine gray
PIL	posterior intralaminar nucleus of thalamus
POL	posterior limiting nucleus of thalamus
PoT	posterior triangular nucleus of thalamus
PPnT	posterior paralaminar nuclei of thalamus
PRC	precommissural nucleus
PRN	pontine reticular nucleus
PRP	prepositus nucleus
PRT	pretectal region
PV	parvalbumin
RE	reuniens nucleus of thalamus
RFP	red flourescent protein
RH	rhomboid nucleus of thalamus
RORB	RAR (retinoic acid receptor) related orphan receptor B
RSP	retrosplenial area
RSPv	ventral retrosplenial cortex
SC	superior colliculus

SCm	superior colliculus, motor-related
SCs	superior colliculus, superficial layers
SGN	supragenicular nucleus of thalamus
SN	substantia nigra
SPF	subparafascicular nucleus of thalamus
SPVO	spinal nucleus of trigeminal, oral part
SSp	somatosensory cortex, primary
SSs	somatosensory cortex, supplementary
TEa	temporal association area
TU	tuberal nucleus
VISpor	postrhinal visual area
VMH	ventromedial nucleus, hypothalamus
WPRE	woodchuck hepatitis virus (WHP) posttranscriptional regulatory element
YFP	yellow fluorescent protein
ZI	zona incerta

List of figures

Supplementary table (Appendix A)

Supplementary figures (Appendix B)

1 Introduction

Innate behaviors in response to relevant stimuli are critical for animal survival. Animals hunt prey, escape from predators, explore novel environments, and orient to stimuli based on complex, multisensorial inputs. Many of these instinctive reactions rely in large part on visual stimuli. Visual input alone has been shown to elicit a selection of innate behavioral strategies such as escape behavior in response to a "looming" stimulus or freezing in response to a "sweeping" stimulus in mice (Yilmaz and Meister, 2013; De Franceschi et al., 2016). These types of behaviors are observed across rodent species (Wallace et al., 2013; Campeau and Davis, 1995; Sewards and Sewards, 2002), and visual threats are also known to elicit analogous neural responses in humans and non-human primates (Almeida et al., 2015; Soares et al., 2017; Soares et al., 2017a; Vagnoni et al., 2015; Vagnoni et al., 2012). Research has linked aberrations in the visual threat response system to human disease and disorders such as PTSD, autism and schizophrenia (Olivé et al., 2018; Terpou et al., 2019; Elsabbagh et al., 2009; Vlamings et al., 2010; Thakkar et al., 2015; Thakkar and Rolfs, 2019), highlighting the translational importance of the underlying circuity. Due to the conserved nature of collicular function, studying the circuitry responsible for regulating visually guided innate behaviors can give us relevant and valuable insights into human brain function and dysfunction.

The superior colliculus, an ancient structure in the mammalian midbrain, plays a vital role in linking such sensory input with activation of motor output. Its contribution to triggering approach and avoidance behavior in rodents has been established for many years (Sahibzada et al., 1986; Dean et al., 1988; Dean et al., 1989; Sparks et al., 1990; Wei et al., 2015; Liang et al., 2015; Basso and May, 2017), and recent evidence shows that cell-type-specific projections from the colliculus are involved in distinct behaviors (Shang et al., 2015; Shang et al., 2018; Hoy et al., 2019; Wei et al., 2015). The identification of these projections and their link to behavior makes the superior colliculus an ideal candidate for studies of the brain-wide consequences of sensory activation.

While great progress has been made in uncovering collicular projections capable of triggering visually guided behaviors, the interactions of the distinct downstream networks and their specific contributions to behavior remain ill-defined. Studies of these circuits in humans have been performed with fMRI (Olivé et al., 2018; Terpou et al., 2019; Meyer et al., 2019; Wang et al., 2020), but the limited spatiotemporal resolution of fMRI makes it difficult to measure activity in smaller brain regions and nuclei; causal relationships are also difficult to assess, as circuits cannot be manipulated directly. Rodent models provide an opportunity to overcome this limitation, as the rodent brain is relatively accessible for in vivo neuronal manipulations, and high-resolution imaging techniques are becoming widely available (Ito and Feldheim, 2018). Previous work in rodents is largely limited to studying well-established mono-synaptic projections, which can be misleading, as we miss the activity of the brain as a whole. Many collicular outputs appear to have the same or a similar role, raising the question of whether they follow independent pathways or converge. Thus, dissecting the multi-synaptic targets of the superior colliculus in a functional context could lead to a better understanding of the coordinated activity of various downstream nodes and their contributions to collicular driven behaviors. Directly manipulating collicular pathways in a mouse model is essential in a translational context, for dissecting these circuits will bring us closer to

understanding related human disease mechanisms and providing novel targets for therapy.

1.1 The superior colliculus: organization

As a major target of retinal outputs, the superior colliculus is uniquely positioned to integrate visual information with other sensory input (Ito and Feldheim, 2018). Its complex laminar structure contains superficial layers, which receive visual inputs with a retinotopic organization. The upper visual field is mapped onto the medial superior colliculus, while the lower visual field is represented by the lateral portion (Dräger and Hubel, 1975; Dräger and Hubel, 1976; Watson, 2012). Ecologically speaking, it stands to reason that in rodents detection of overhead predators activates the medial superior colliculus, triggering defensive behavior, while detection of prey can activate the lateral portion and trigger appetitive behavior (Comoli et al., 2012; Yilmaz and Meister, 2013). This medial-lateral collicular organization is conserved in non-human primates and humans (DuBois and Cohen, 2000; Schneider and Kastner, 2005; Katyal et al., 2010; Cynader and Berman, 1972). Projections from the superficial superior colliculus target a large number of areas throughout the brain (Figure 1). The deeper layers of the colliculus receive multimodal (somatosensory, auditory, and visual) sensory input (Watson, 2012; May, 2006). Sensory information from the colliculus is routed to numerous downstream nuclei and cortical regions, which induce motor output (Kamishina et al., 2008; Wei et al., 2015; Zhou et al., 2018; Mitchell et al., 1988; Evans et al., 2018).

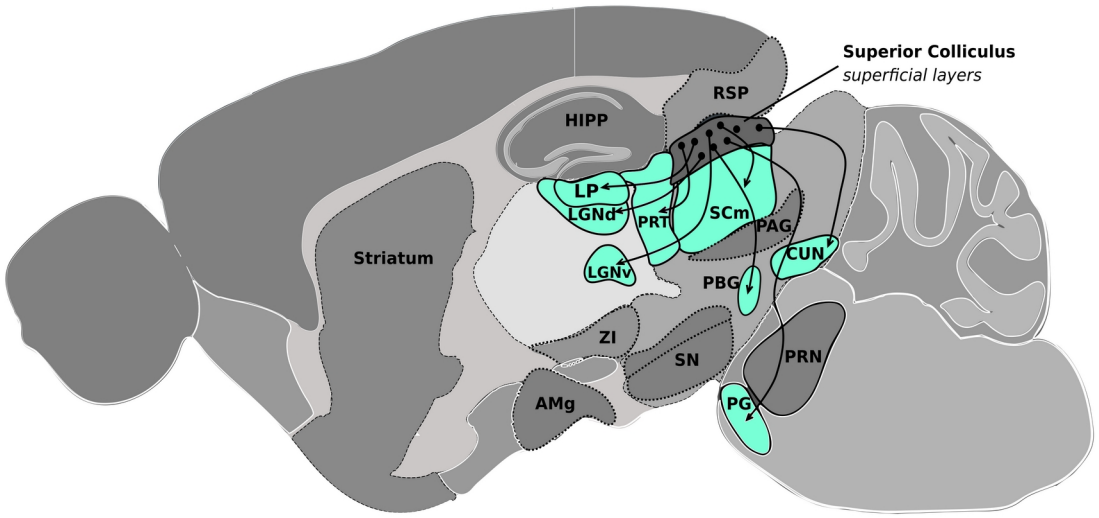

FIGURE 1 | Projections from the superficial layers of the superior colliculus. Sagittal schematic diagram of the complex mono- (light blue areas) and multi-synaptic (gray, labeled areas) projections of the superficial layers of the superior colliculus throughout the rodent brain. Mono-synaptic outputs: SCm superior colliculus motor-related, LP lateral posterior nucleus of thalamus, LGNd lateral geniculate nucleus dorsal part, LGNv lateral geniculate nucleus ventral part, PRT pretectal region, CUN cuneiform nucleus, PBG parabigeminal nucleus, PG pontine gray. Multi-synaptic outputs: HIPP hippocampus, RSP retrosplenial area, , PAG periaqueductal gray, SN substantia nigra, ZI zona incerta, PRN pontine reticular nucleus, AMg amygdala, striatum.

1.2 Cell-types of the superior colliculus and their projections

Recent studies have characterized distinct genetically-identified cell types in the superficial layers of the colliculus, which have specific projection patterns and respond to specific visual stimuli (Figure 2). The four widely-recognized cell-types are termed wide-field, narrow-field, horizontal, and stellate cells based on their dendritic morphology (Gale and Murphy, 2014). Transgenic mouse lines have been identified in which Cre recombinase is expressed in each cell-type based on genetic identity. Wide-field neurons are positive for NTSR (neurotensin receptor) and are therefore labeled with Cre in the NTSR-GN-209-Cre mouse line. They respond to small stimuli moving within a large field, and project solely to the lateral posterior nucleus of the thalamus (LP; Gale and Murphy, 2014; Wei et al., 2015; Gerfen et al., 2013). Narrow-field cells, labeled in the Grp-KH288-Cre mouse line, project to the deep layers of the superior colliculus and to the parabigeminal nucleus (PBG). They respond to slow-moving stimuli and have small receptive fields. Horizontal cells, labeled in the GAD2-Cre line, are inhibitory projection neurons that respond to large, stationary or rapidly-moving stimuli, and target the lateral geniculate nucleus of the thalamus (LGN) and PBG (Gale and Murphy, 2014). Stellate cells, labeled in the Rorb-Cre mouse line, albeit non-specifically (Gale and Murphy, 2018), have small receptive fields and respond to small stimuli. They project to the LGN and PBG as well. In addition to these four cell-types, a population of parvalbumin-positive (PV+) cells displays heterogeneous morphological and electrophysiological properties suggestive of a mixed population of narrow-field, stellate, and horizontal cells (Shang et al., 2015; Villalobos et al., 2018). Projections of excitatory PV+ (parvalbumin) neurons target the LP, PBG, and the pontine gray (PG; Shang et al., 2015; Shang et al., 2018).

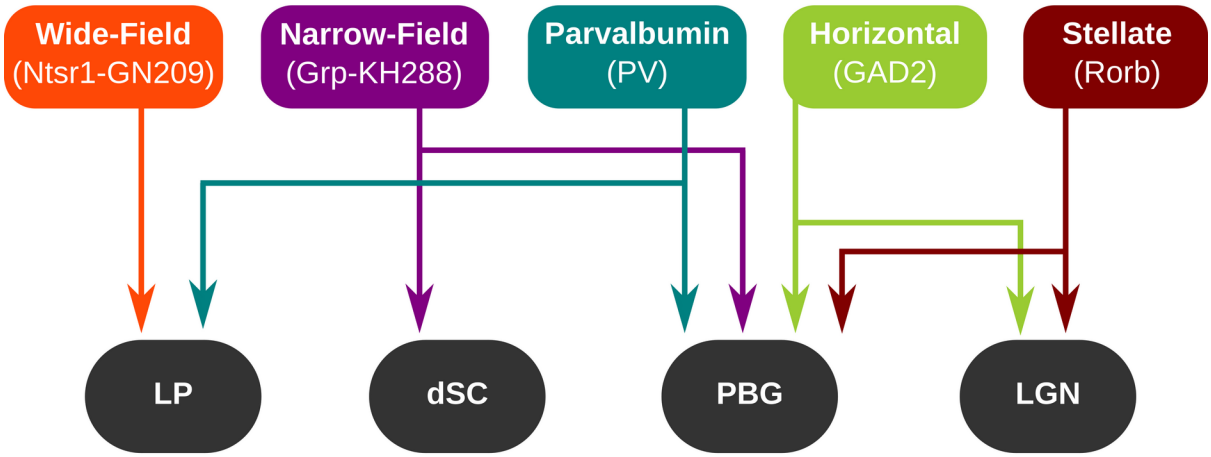

FIGURE 2 | Cell-types of the superficial layers of the superior colliculus, their genetic labels and projections. Simplified scheme of the major projections of collicular cell-types. LP lateral posterior nucleus, dSC deep layers of superior colliculus, PBG parabigeminal nucleus, LGN lateral geniculate nucleus.

1.3 Cell-type specific behavior

Isolation of these anatomical projections has allowed for characterization of their role in mediating innate behaviors. For example, optogenetic activation of the LP pathway elicits freezing behavior, and activation of the PBG projection induces escape behavior (Wei et al., 2015; Shang et al., 2018). Corresponding flight and arrest behaviors have been

observed upon presentation of looming (representing an approaching predator) and sweeping (representing a passing predator) visual stimuli respectively (Yilmaz and Meister, 2013; De Franceschi et al., 2016). Thus, optogenetic activation of these pathways can act as a reliable proxy for visual stimuli simulating predators. Despite progress in associating defensive behaviors with these specific projections, the particulars of the circuits governing cell-type specific behaviors are not well-defined.

In recent work, Sans-Dublanc et al. (2020) explored the distinct contributions of collicular cell-types to avoidance behavior by optogenetic activation of four specific genetically defined cell populations in the superficial superior colliculus: 1) excitatory CAMKII-expressing neurons, to establish the effect of general excitatory activity; 2) NTSR-expressing (wide-field) neurons targeting the LP; 3) PV-expressing neurons consisting of excitatory projections to the LP, PBG, and PG and some local interneurons; 4) and GAD2-expressing inhibitory (horizontal) neurons and interneurons projecting to the LGN and PBG. To limit expression of channelrhodopsin-2 (ChR2), a light-sensitive ion channel, to these cell-types, transgenic mouse lines expressing Cre in NTSR, GAD2, and PV neurons (*NTSR-GN209-Cre, Gad2-Cre, PV-Cre*) were crossed with a Cre-dependent ChR2-YFP (yellow fluorescent protein) reporter line *(Ai32).* This resulted in three mouse lines expressing ChR2 in the specific collicular cell-type. To target the CAMKII population, an adeno-associated virus (AAV) carrying ChR2 was delivered to the superficial superior colliculus in CAMKII mice. Histological analysis confirmed ChR2 expression in each mouse line (Figure 3B). Controls were Cre-negative litter mates.

To allow for optical stimulation of these specific populations, optic fibers were implanted above the dorso-medial portion of retino-recipient layers in the superior colliculus based on previous work showing cell bodies of these neurons to be located in this region (Shang et al., 2018; Shang et al., 2015; Gale and Murphy, 2014). Behavioral testing consisted of an open field test, in which the optic fiber was attached to a blue-light laser via a patch cable, and mice were allowed to freely explore an arena. Whenever the mouse crossed the center of the arena, the laser was manually triggered (Figure 3A). Repeated activation of the distinct collicular cell-types was shown to elicit specific, consistent behavioral responses. For example, stimulation of CAMKII neurons led to prolonged freezing behavior (median duration: 9.21 s, IQR=[8.02, 12.65]; Figure 3C-D, F). In contrast, stimulation of GAD2 neurons resulted in a speed increase during stimulation and accompanying change in direction (Figure 3C-E, G), while PV animals tended to escape to the corners of the arena with a decrease in speed (Figure 3C-E, H). Control mice did not show any change in behavior during stimulation.

1.4 Activation of collicular NTSR neurons elicits stopping behavior

Of importance to this project is the response of NTSR x ChR2 mice, which express ChR2 in all NTSR neurons. In the superior colliculus, NTSR is expressed in wide-field neurons alone, allowing us to target the population of wide-field neurons projecting to the LP. Upon optogenetic stimulation of collicular NTSR neurons in NTSR x ChR2 mice, the mice displayed marked and sudden stopping behavior. The period of locomotive arrest was of shorter duration than that of the CAMKII mice (median duration 1.69 s, IQR=[1.42, 1.95], Figure 3C-D, F). With this added insight into behaviors linked to a specific cell type, the next focus was examining the downstream networks modulating these behaviors.

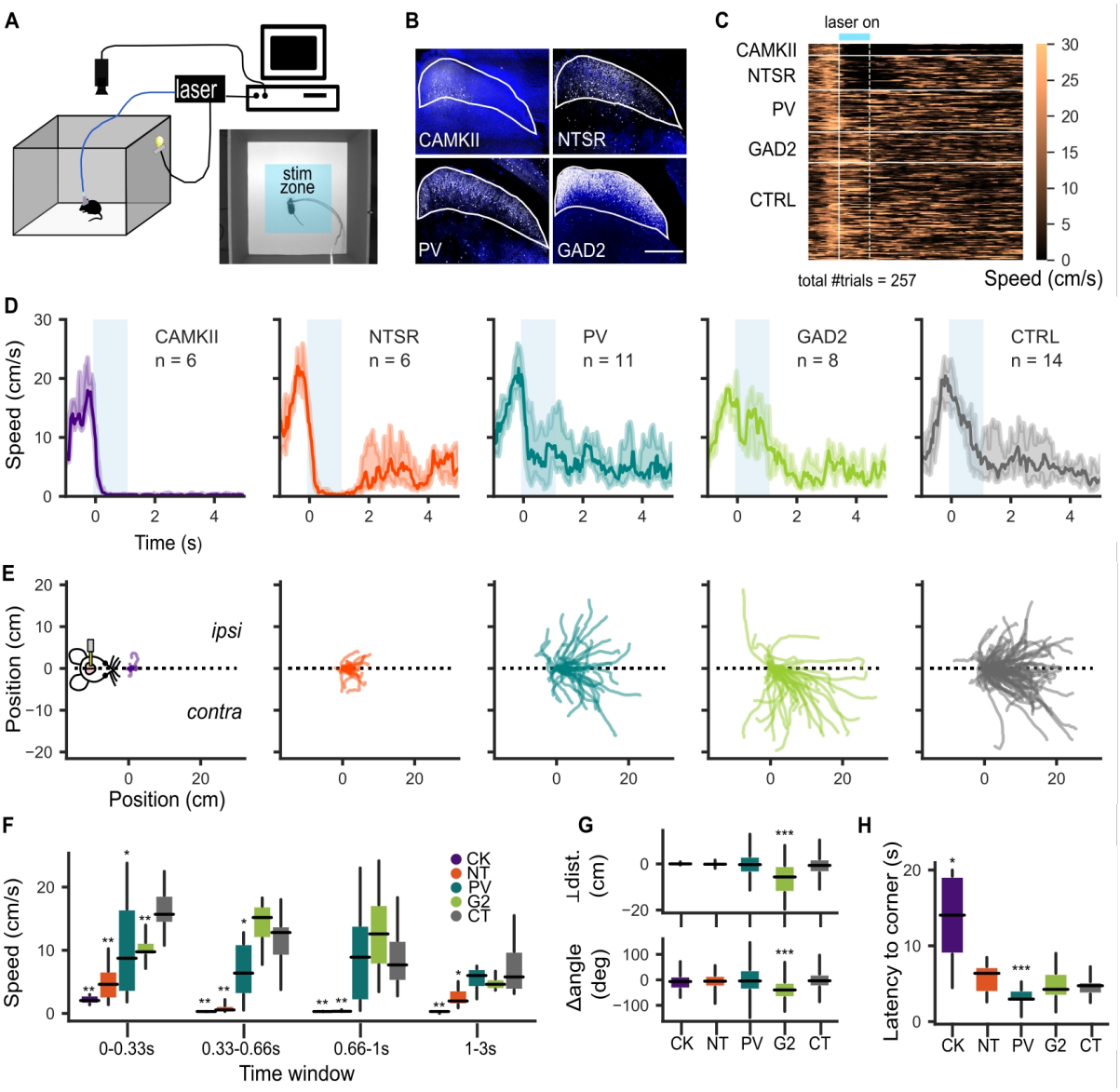

FIGURE 3 | Cell-type specific activation of the superior colliculus elicits distinct behaviors (Sans-Dublanc et al., 2020). A. Schematic diagram of open field set-up for optogenetic stimulation. Still frame from video recording shows zone (blue rectangle) in which laser is triggered manually when the mouse runs across. **B.** Histological confirmation of ChR2 expression in the superior colliculus in each mouse line (coronal sections; scale bar, 500 μm). **C.** Heatmap showing speeds prior to, during, and after stimulation for each trial. Horizontal white lines split trials per mouse line. Solid and dashed white vertical lines represents stimulation onset and offset respectively. **D.** Speed traces over all stimulation trials for each mouse line. Bold line indicates median speed, and shaded area shows the IQR. Blue shaded rectangle indicates 1 s stimulation. **E.** Trajectories of mice during 1 s stimulus. Traces were aligned based on the initial body position angle. CAMKII: n=6, 14 trials, NTSR1: n=6, 41 trials, PV: n=11, 50 trials; GAD2: n=8, 43 trials; CTRL n=8, 77 trials. **F.** Comparison of speeds of each mouse line during time window indicated. Stimulation onset/offset was 0-1 s. **G.** Body position at end of stimulation, indicated as perpendicular distance (top) and change in angle (bottom) from x-axis. **H.** Latency to reach corner after stimulation, quantified for each mouse line. Data represents averages over mice, with the exception of G which represents averages over trials. Significance between controls and each mouse line was tested using Mann-Whitney U-test (alpha = 0.05). **F-H**. Box-and-whisker plots show median, IQR and range. * $P < 0.05$, ** $P < 0.01$, *** $P < 0.001$.

1.5 Whole-brain mapping shows broad networks of distinct functional nodes activated by cell-type specific stimulation

To investigate whole-brain activity when collicular cell types are activated, optogenetic stimulation was paired with simultaneous whole-brain functional ultrasound imaging (fUSi) in awake, head-fixed animals. fUSi is a novel imaging modality, which is based on Doppler ultrasound and allows real-time whole brain recordings in freely moving rodents with high spatiotemporal resolution (~100μm^3, 100ms; Urban et al., 2014; Macé et al., 2018). An additional advantage of fUSi is the compact size of the set-up, which allows for concurrent manipulations, such as optogenetic activation, during recording. fUSi imaging during optogenetic stimulation was performed for each of the four mouse lines (Sans-Dublanc et al., 2020). The functional data, given by changes in blood volume across the microvasculature of the brain, were co-registered with the Allen Mouse Brain Reference Atlas to reveal brain areas activated by optogenetic stimulation of the specific collicular cell types.

Results showed that activation of each cell-type modulated activity of between 68 and 193 brain areas scattered across the cortical plate, midbrain, cerebellum, and thalamus. Activation of the motor layers of the superior colliculus was observed in all mouse lines, as was activity in the dorsal periaqueductal gray (dPAG) and zona incerta (ZI), both of which are known to play a role in defensive behavior (Assareh et al., 2016; Carrive, 1993; Wang et al., 2019). While some overlap existed, cell-type specific stimulation activated largely distinct downstream networks. Of note, activity in a greater number of brain areas seemed to be indicative of a more exaggerated behavioral response. Overall, these findings indicate that collicular defensive behaviors are mediated by incredibly complex, distinct networks which share some common nodes. Further evaluation of the contribution of functional nodes to behavioral modulation tied to collicular cell types remains our focus of study.

In NTSR x ChR2 mice, fUSi recordings during optogenetic stimulation of NTSR collicular neurons showed activity in several nodes of interest (Figure 4A-B). As expected, activity in the LP, the mono-synaptic target of the wide-field neuron projection, was confirmed. High responses were also observed in several areas which have never been associated with collicular-driven innate behaviors. Two such nodes are known to receive projections from the LP, namely the tail of the caudoputamen (CPu; Takada et al., 1985; Redgrave et al., 2010) and the postrhinal visual area (VISpor; Figure 4A-C; Tohmi et al., 2014; Beltramo and Scanziani, 2019; Bennett et al., 2019; Nakamura et al., 2015).

1.6 fUSi identifies novel functional node in wide-field neuron collicular circuit

Of particular interest, activity was also identified in a group of thalamic areas adjacent to the medial geniculate complex, referred to here as the posterior paralaminar nuclei (PPnT; Figure 4A-B; Linke, 1999), which have not been previously implicated in the NTSR collicular neuron downstream pathway. A mono or di-synaptic connection from the retino-recipient layers of the SC to the PPnT has not been established in mice (Figure 4C). This group of nuclei includes the suprageniculate (SGN), posterior limiting (POL), posterior triangular (PoT), and posterior intralaminar (PIL) nuclei (Figure 4D; Winer and Morest, 1983; Ledoux et al., 1987; Winer and Larue, 1988).

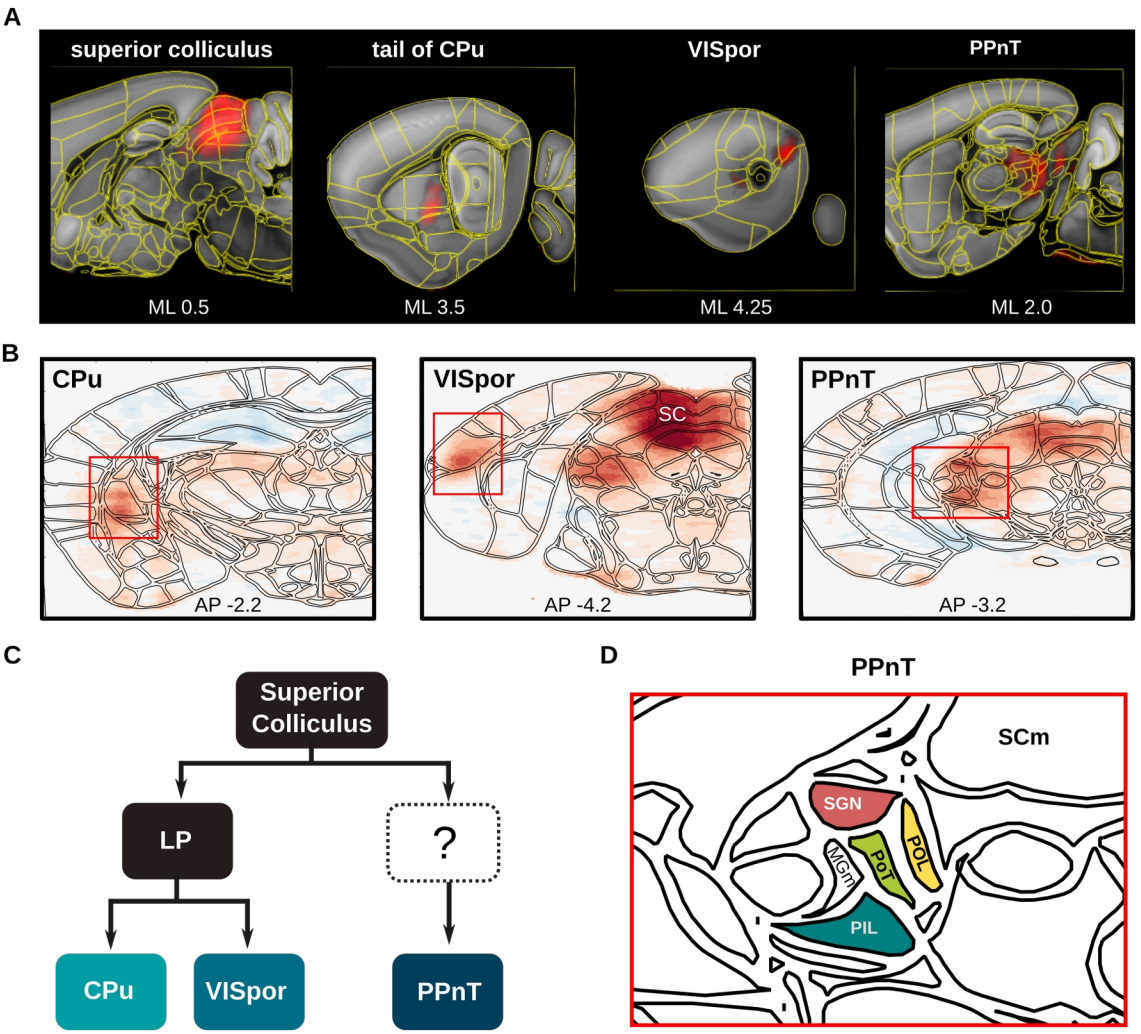

FIGURE 4 | Whole brain mapping shows distinct functional nodes activated by NTSR neuron stimulation. A. Raw sagittal fUSi images of key brain regions active during optogenetic stimulation of NTSR neurons in the superior colliculus. **B.** Coronal sections of normalized response to optogenetic stimulation of NTSR collicular neurons in regions of interest co-registered and aligned to the Allen Mouse Brain Reference Atlas. Red box surrounds labeled brain region of interest. **C.** Scheme illustrating collicular connectivity of regions identified in fUSi. **D.** Enlargement of PPnT from Panel B, showing delineation of nuclei (colored regions): SGN suprageniculate nucleus, PoT posterior triangular nucleus, POL posterior limiting nucleus, PIL posterior intralaminar nucleus. Also shown: SCm superior colliculus, motor-related, MGm medial division of medial geniculate complex.

Inputs to the PPnT are thought to be multi-modal with auditory, visual, and somatosensory origin (LeDoux et al., 1984; Peschanski, 1984; Hicks et al., 1986; Arnault and Roger, 1987; Ledoux et al., 1987; Bordi and LeDoux, 1994; Bordi and LeDoux, 1994; Benedek et al., 1997; Linke, 1999). Research in rats suggests that the PPnT receive projections from the superior colliculus (Linke, 1999; Tanaka et al., 1985), and project in turn to the amygdala, basal ganglia (Moriizumi and Hattori, 1992; Shammah-Lagnado et al., 1996; LeDoux et al., 1985), and inferior colliculus (Senatorov and Hu, 2002; Winer et al., 2002). The PPnT appear to transmit sensory stimuli to the amygdala, and this projection has been suggested to play a role in auditory associative

learning (LeDoux et al., 1986; Iwata et al., 1986; LeDoux et al., 1988; Ledoux and Muller, 1997; Romanski and LeDoux, 1992; McEchron et al., 1995; McEchron et al., 1996), but not maintenance (Campeau and Davis, 1995; Campeau and Davis, 1995) in fear conditioning paradigms. To date, the link between the PPnT and innate behavior in a visual context remains largely unexplored.

1.7 Aim of the project: examination of the connectivity of the PPnT and its role in collicular-driven defensive behavior

While previous literature supports the notion that the PPnT could play a role in collicular-mediated defensive behaviors in mice, a direct link has yet to be established. This is due to the paucity of studies in a mouse model as well as the focus on conditioned behaviors and auditory functions of the PPnT in previous work. Circuitry studies have been largely limited to rat and cat models. In mice, there is preliminary evidence for projections from the PPnT to the amygdala and auditory cortex (Keifer et al., 2015; Asede et al., 2015).

We seek to shed light on the PPnT's connectivity and functional role in visually-evoked innate behavior in a mouse model. We provide a first approximation of inputs to the PPnT using retrograde viral tracing techniques. To examine the contribution of the PPnT to arrest behavior, we optogenetically stimulate NTSR collicular neurons while simultaneously inhibiting the PPnT chemogenetically with Designer Receptors Exclusively Activated by Designer Drugs (DREADDs) in an open field behavioral paradigm. Our study reveals that the PPnT may play a role in modulating habituation to repeated presentation of a stimulus, rather than active involvement in the execution of collicular behavior.

2 Methods

A general experimental timeline is detailed in Figure 5.

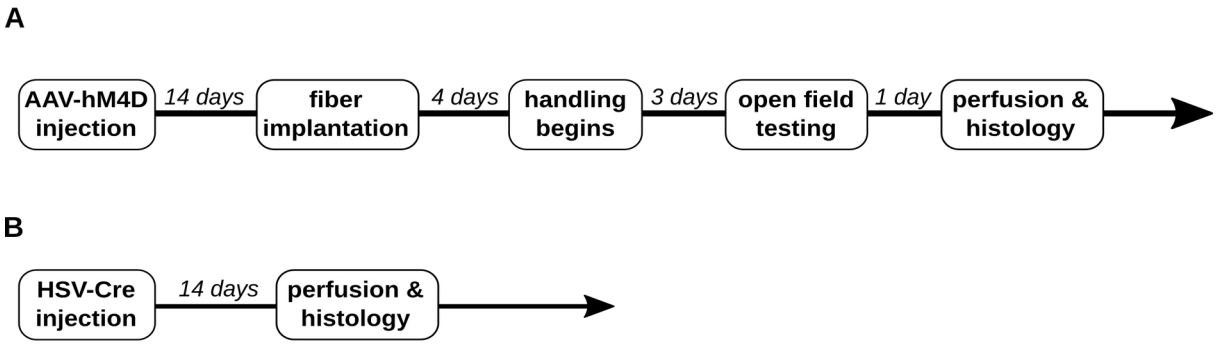

FIGURE 5 | General experimental timeline. A. Timeline of optogenetic open field behavior experiments. **B.** Timeline of retrograde viral tracing experiment.

2.1 Experimental model and subjects

Adult transgenic mice (8 weeks old for viral injections, 11 weeks for behavioral experiments) of either sex were used in the experiments. We used three mouse lines in the project: *NTSR1-GN209Cre* (n=16), *NTSR1-GN209Cre x Ai32* (n=24 Cre-positive, n=8 Cre-negative), and *Ai9* (n=1). *NTSR1-GN209Cre* (Genset: 030780-UCD) mice, hereafter referred to as NTSR1-Cre, express Cre recombinase in *NTSR1-GN209*-expressing neurons (Gerfen et al., 2013). *Ai32* (JAX: 012569) is a reporter line expressing ChR2-YFP in the presence of Cre recombinase. *NTSR1-GN209Cre x Ai32,* a cross between *NTSR1-GN209Cre* and *Ai32* mice and hereafter referred to as NTSR x ChR2, express ChR2 fused to YFP in *NTSR1-GN209*-expressing neurons (Madisen et al., 2010). *Ai9* (JAX: 007909) is a reporter mouse line expressing tdTomato fluorescence upon Cre-mediated recombination.

The mice were maintained on a 12-hour light/dark cycle and given *ad libitum* access to sterilized food (14% protein maintenance diet) and water. Nesting and bedding material were provided. Experiments were performed during the light phase. The animals were socially housed until fiber implantation, after which they were individually housed to minimize risk of damage to the animal and the optical fiber. All animal procedures were carried out in accordance with the ethical guidelines of KU Leuven and the European Communities Guidelines on the Care and Use of Laboratory Animals (004–2014/EEC, 240–2013/EEC, 252–2015/EEC).

2.2 Viral Injections

2.2.1 Viral vectors

NTSR x ChR2 experimental mice (n=17) were injected in the PPnT with 200 nl of AAV2-hSyn-hM4D(Gi)-mCherry (Addgene, 50475) for expression of the inhibitory DREADD human Gi-coupled M4 muscarinic receptor (hM4D) fused with mCherry under control of the human synapsin promoter. NTSR x ChR2 control mice (n=7) were injected in the

PPnT with 200 nl of AAV2-hSyn-EYFP (UNC vector core, AV4376E) for expression of YFP as a reporter. For expression of ChR2 in a targeted population of wide-field (NTSR collicular) neurons, we injected 200 nl of AAV2-EF1a-DIO-hChR2(E123T/T159C)-p2A-EYFP-WPRE (UNC vector core, AV5468C) into the superficial superior colliculus of NTSR1-Cre mice (n=16; Mattis et al., 2011). We also injected NTSR1-Cre mice with AAV-hM4D into the PPnT, as detailed above. The tdTomato mouse (n=1) was injected with a modified HSV-cre (hEF1-cre HT) for retrograde viral tracing.

2.2.2 Surgical preparation

Animals were anesthetized via intraperitoneal injection of ketamine (75 mg/kg body weight) and medetomidine (1 mg/kg) in saline. Anesthetic depth was verified by absence of the pedal reflex. The head was disinfected and the fur covering the skull removed. The mice were head-fixed in a stereotaxic device (Narishige, SR-5N) and surgery performed on a heated pad (37°C) to preserve stable body temperature. Eye ointment (Dura Tears, Novartis, 288/28062-7) was applied to the eyes to prevent dryness, and a local anesthetic (Lidocaine 0.5%, 7 mg/kg) was injected subcutaneously. An incision was made along the midline to expose Lambda and Bregma landmarks for stereotaxic measurements. A small craniotomy was made above the injection site using gentle rotation of a needle to penetrate the skull (BD Micro-Fine + 8 mm x 0.25 mm).

2.2.3 Injection

Viruses were loaded in a sharp, pulled-glass micropipette (Wiretrol II capillary micropipettes, Drumond Scientific, 5-000-2005; Sutter Laser-Based Micropipette Puller, P-2000) with an open tip of 30 µm and mounted on an oil-based hydraulic micromanipulator (Narishige MO-10) for stereotaxic injections. The micropipette tips were coated with DiD (Thermo, D7757) to mark the injection sites. 100 nl of virus was injected at each depth with 5-minute intervals between each injection.

Anterior-posterior (AP) coordinates are measured from Bregma, medial-lateral (ML) coordinates are measured from midline, and dorsal-ventral (DV) coordinates are measured from the surface of the skull. Injections were consistently made in the left hemisphere. AP and ML coordinates were based on the Allen Mouse Brain Atlas (Bakker et al., 2015) and the Paxinos atlas was used for DV coordinates (Franklin, 2019). We used a standard Lambda-Bregma distance of 4.7 mm and maximal lateral distance from midline of 5.0 mm. To account for variation in brain size, we applied a correction factor (actual / standard) when actual measurements were outside a ± -0.1 mm margin of error. PPnT coordinates were AP: -3.0 to -3.4 mm; ML: 1.8 to 2.0 mm; DV: -3.4 and -3.3 mm. For AAV-ChR2 injections to the medial retino-recipient layers of the superior colliculus, the following coordinates were used: AP: -3.6 to -3.8 mm; ML: 0.3 mm; DV: -1.3 and -1.2 mm.

Following injection, the incision was closed using Vetbond tissue adhesive (3M, 1469) and Antisedan (atipamezole, 1 mg/kg) was administered intraperitoneally. Mice were allowed to recover on a heating pad and given access to soft food and water containing antibiotics (emdotrim, ecuphar, BE-V23552). To ensure adequate viral expression, we waited two weeks before sacrificing animals for the viral tracing experiment and three weeks before performing behavioral experiments.

2.3 Fiber optic cannulae implantation

After mice recovered from the viral injections, we performed headposting and fiber optic cannulae implantation into the superior colliculus to allow for optogenetic activation. Surgical preparation followed the same procedure outlined in Section 2.2.2. The lateral and posterior muscles attaching to the skull were pushed back and Vetbond adhesive applied around the open skin incision. A titanium headpost was secured to the animal's skull using Dental acrylic (Super-Bond C&B) mixed in a cooled ceramic tray. The headpost was used to align the head during fiber implantation and to stabilize the mouse while attaching the patch cable to the optic fiber in behavior experiments.

A craniotomy was performed to expose the cortex above the implantation site. We used a dental drill to thin the skull; the thinned piece of skull was then removed with fine forceps. The fiber optic cannula (Doric lenses, MF1.25, 200/245-0.37, FLT) was inserted into a probe holder and connected to a stereotaxic arm for implantation. Coordinates for the fiber entry on the surface of the brain were: AP: -3.1 to -3.7 mm; ML: 1.5 mm contralateral to the virus injection site. The fiber was inserted 1.9 mm into the brain at 54° for a final tip placement above the superior colliculus at AP: -3.1 to 3.7 mm; ML: 0 mm; DV: -1.1 mm (see Figure 7B for example). The angled implantation strategy increases the area of the superior colliculus that can be illuminated by the stimulation and facilitates access to the deeper layers of the superficial superior collicular where cell bodes of wide-field neurons are found without damaging the layers above. The fiber was secured with dental cement. Following the procedure, the animals were individually housed in clean cages to aid recovery and to avoid damage to the head post and fiber from cage mates. Mice were provided access to a heating pad for 24 hours post-surgery and treated with painkillers (Buprenorphine 0.2 mg/kg I.P.) and antibiotics (Cefazolin 15 mg/kg I.P.) for up to 3 days post-surgery depending on the animal's condition. Behavioral experiments were performed at least 4 days after fiber implantation to allow for total recovery.

2.4 Optogenetic open field test

2.4.1 Open field set-up and data acquisition

The 20-minute open field behavioral tests were performed in a custom-made square wooden box (W: 50 cm x L: 50 cm x H: 36 cm) (Figure 6B). A lamp was positioned overhead and directed toward a wall to provide dim ambient light (~50 lux). A video of the test was acquired with a Firefly MV camera fixed 53 cm above the arena center and recorded as M-JPEG files with FlyCap2 Image Acquisition application (37,000 frames; frame rate: 30 frames per second (fps); JPEG compression quality 75). For optogenetic activation, we used a blue light (473 nm) DPSS laser system (Laserglow Technologies, R471003GX) connected to a patch cord. Custom MATLAB codes were used to deliver a 1-second stimulation at 20 Hz with 2 ms pulse width. This frequency was chosen based on previous reports indicating that firing rates of natural visual responses in the superior colliculus is 20 Hz (Wei et al., 2015). Before experiments, the laser output was tested at 20 Hz and set at 0.2 mW.

Mice were habituated to handling beginning at least 3 days prior to behavioral testing. Just prior to recording, we connected the patch cord to the fiber optic cannula of the mice via a rotary joint (Thorlabs, RJPFL2) to allow free movement. The animal was then

placed into the open field and allowed to freely explore the arena. After a 2 minute period of acclimatization, the laser was manually triggered mid-stride when the mouse crossed the center (Figure 6B). A small LED indicator attached to the box itself was also activated whenever the laser was triggered, and this visual cue was used in the video tracking to verify the precise time of stimulation. Each 1 s stimulation is referred to as a trial. We waited at least 30 seconds between stimulation trials, and each mouse underwent approximately 15 trials in a 20-minute session.

2.4.2 Experimental Design

Experimental animals expressed inhibitory DREADD receptor hM4D in the PPnT while non-DREADD control animals expressed a reporter gene for YFP in the PPnT. Both groups underwent identical surgical procedures, housing conditions, open field behavioral testing, and treatment with clozapine-N-oxide (CNO), the hM4D actuator. hM4D is expressed in the cell bodies and axons of neurons, and CNO administration activates the receptor, leading to hyperpolarization and suppression of electrical activity of hM4D-expressing cells (Armbruster et al., 2017). Both groups received saline vehicle control and ligand injections to control for non-specific effects of CNO metabolism (Goutaudier et al., 2019).

Behavioral testing consisted of five open field sessions. Sessions 1 to 4 were performed at 48-hour intervals with Session 5 following one week later (Figure 6A). Environmental noise and light pollution were kept at a minimum. Saline or CNO (1.0 mg/kg body weight) was injected intraperitoneally 30-40 minutes prior to each test (Figure 6A). In Session 1, saline was administered to all animals prior to the open field test to establish a baseline of behavior due to collicular activation with the laser. In Session 2, 48-hours later, animals received an injection of CNO to locally inhibit the cells in the PPnT in hM4D-expressing mice. In YFP-expressing control mice, no PPnT inhibition occurred. Sessions 3 to 5 featured saline injections for all animals in order to investigate recovery of the behavioral responses.

The metabolism of CNO to clozapine and the potential for its binding to endogenous receptors is an important consideration in CNO-based DREADD studies (Mahler and Aston-Jones, 2018; Gomez et al., 2017; Manvich et al., 2018). Clozapine reaches peak CSF concentrations at 2-3 hours after CNO administration (Gomez et al., 2017), thus we began our behavioral tests 30-40 minutes after administration, at which time point the ratio of clozapine to CNO in mice has been shown to be 7.4% (Manvich et al., 2018). Separating behavioral sessions by 48 hours ensures clearance of CNO and its metabolites.

2.4.3 Data Extraction and Processing

Video recordings of behavior testing were analyzed using DeepLabCut open source software, which performs 3D pose estimation based on deep learning methods (Mathis et al., 2018). A training dataset was created by manually labeling various body parts of the mouse, such as the nose, tail, and ears for 200 video frames (Nath et al., 2019). The network was trained, evaluated, and used to assign labels to video frames automatically based on a feature-extracting deep learning algorithm (Figure 6C, Video S1; all video links and descriptions can be found in Table S1). DeepLabCut yielded a .csv file with x/y label positions in pixels for every frame of each video as well as a confidence score (Mathis and Mathis, 2020). Positional data of the base of the tail was used to

convert the animal's position to velocity (expressed in cm/s) based on a transformation factor incorporating the pixel to distance ratio.

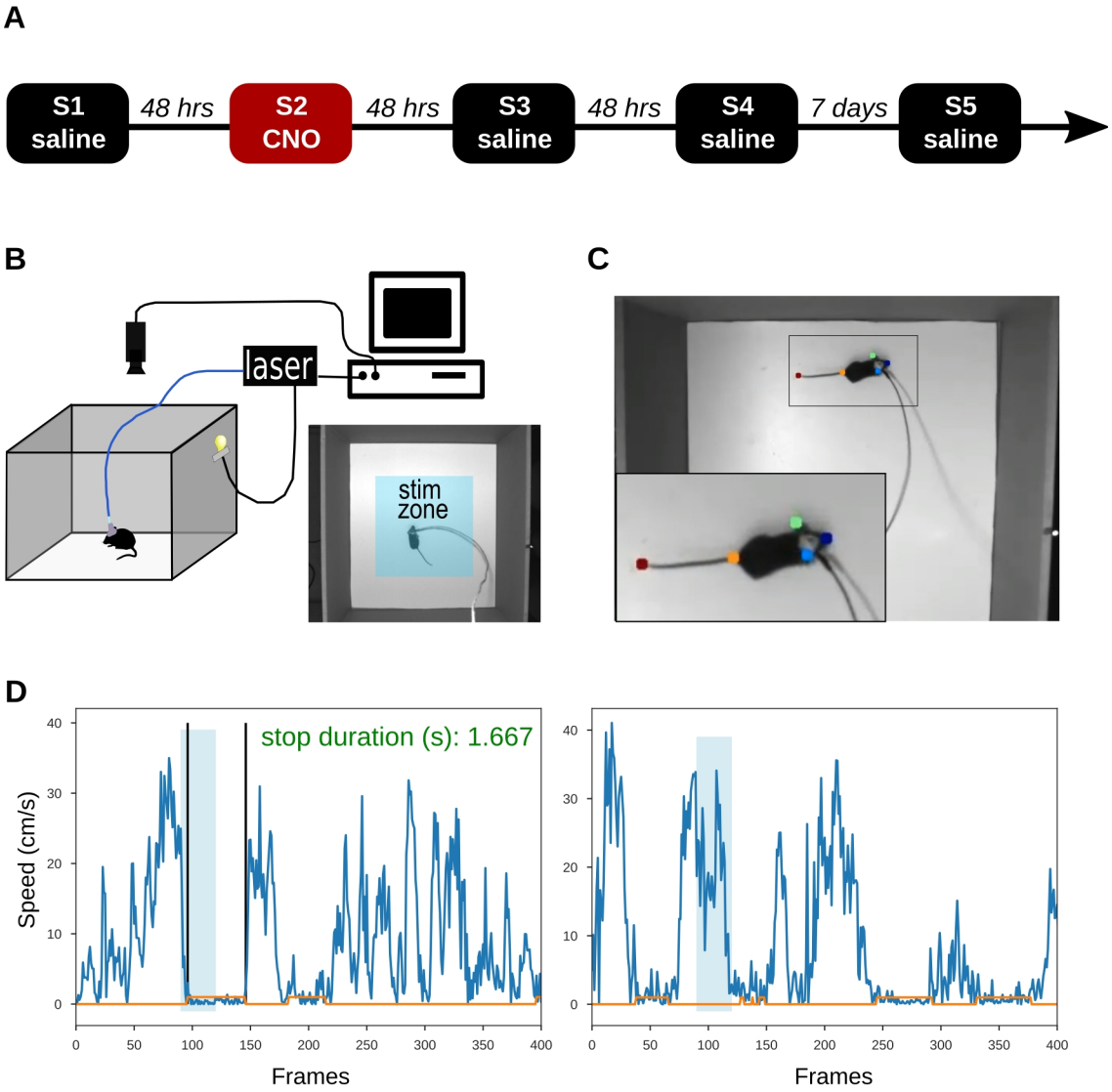

FIGURE 6 | Optogenetic open field experimental set-up and data acquisition. **A.** Timeline of five sessions (S) of behavioral testing with indication of saline or CNO injection. **B.** Schematic diagram of open field set-up for optogenetic stimulation consisting of custom square box, fiber coupled to a blue-light laser, overhead camera, and LED indicator. Still frame from video recording shows zone (blue rectangle) in which laser is manually triggered when the mouse crosses. **C.** Example frame from video recording showing labeled markers (nose, ears, tail base, and tail end) assigned by DeepLabCut. The x/y position of each marker was extracted for every video frame. **D.** Example speed traces for two trials showing extracted speed (cm/s) plotted over recorded video frames (frame rate: 30 fps). Trials were selected from a mouse in the hM4D group in Session 1 (left) and Session 2 (right) and show a trial with a stopping episode (left) and a trial with no stopping (right). Shaded blue rectangle indicates 1 second stimulation. Whenever speed falls under 1.5 cm/s threshold, the orange horizontal line is elevated. This is considered a stopping episode if the duration is > 10 frames (0.33 sec) and the episode begins during the stimulus. If a stopping episode meets the criteria, black vertical lines indicate onset and offset of the episode and the stop duration is calculated and listed in green.

Frames corresponding to optogenetic stimulation were extracted using custom Python code based on the presence or absence of the LED indicator. For each trial, speed vectors consisting of the extracted speeds from 2 seconds preceding the stimulation to 8 seconds post-stimulation were compiled into a data frame. Speed during stimulation in each trial was calculated as the mean of the speed over 20 frames (0.67 s) starting halfway through the stimulation. Each trial was assigned a Boolean value based on the presence or absence of a stopping episode during the stimulation, which was defined as a speed of <1.5 cm/s for at least 0.33 s. This threshold was verified graphically (Figure 6D). The Boolean True/False values were then used to calculate the stopping probability of mice over trials and over sessions. Plots for data visualization were generated using custom Python scripts. Video clips included in Supplementary Material were compiled using Windows Video Editor software.

2.5 Immunohistochemistry

After termination of behavioral experiments, mice were anesthetized with concentrated ketamine (200 mg/kg) and xylazine (30 mg/kg) and transcardially perfused with 1x phosphate-buffered saline (PBS) and 4% paraformaldehyde (PFA, HistoFix, Roche). The animals were decapitated, and brains removed and post-fixed overnight in PFA at 4°C. Specimens were stored in PBS at 4°C until histochemical analyses were performed.

Brains were mounted in 1.5% agarose and sections of 100 or 200 µm were sliced on a vibratome (Leica VT1000 S). Sections were collected in 1 x PBS. All brains were incubated with DAPI (Roche, 10236276001, 1:2000) to stain nuclei for visualization of macroscopic brain structures. Immunofluorescent staining was performed to amplify signals from fluorescent proteins. Brains were first incubated in a blocking buffer (1x PBS, 0.3% Triton X-100, 10% Donkey serum) at room temperature for an hour. Then, slices were incubated with primary antibodies in blocking buffer overnight at 4°C. The following day, slices were washed 3 times for 20 minutes in 1x PBS, 0.3% TritonX-100 and then incubated in secondary antibodies in blocking buffer overnight at 4°C. Primary antibody rabbit anti-GFP (Thermo Fisher, A-11122, 1:1000 antibody:solution) and secondary antibody Alexa488 donkey anti-rabbit (Thermo Fisher, A21206, 1:1000) were used to amplify fluorescence from ChR2-YFP-positive cells. Primary antibody chicken anti-RFP (Thermo Fisher, 1:1500) and secondary antibody Cy3 donkey anti-chicken (Thermo Fisher, 1:500) were used to amplify signals from m-Cherry in hM4D DREADD-expressing cells and for the viral tracing experiments in tdTomato mice. Following secondary antibody incubation, sections were washed 3 times for 20 minutes in 1x PBS, 0.3% TritonX-100 and once in 1x PBS. Sections were then mounted on glass slides and covered with mounting medium (Dako, C0563) and a glass coverslip.

Slides were scanned with a wide-field fluorescence microscope (Olympus MVX10) to verify the location of the injections, fiber implant, and viral expression in each animal. Images were acquired using a ToupCam 5.0 MP CCD camera and Toupview acquisition software. Select examples were scanned under a confocal microscope (Zeiss LSM 710) using a 10x objective (plan-APOCHROMAT 0.45 NA, Zeiss). Histological images were aligned to the coronal Allen Mouse Brain Atlas using the Allen Institute SHARP-Track MATLAB user interface (Shamash et al., 2018).

2.6 Statistical Analysis

Statistical analyses were performed in Python. Data are presented as mean ± standard deviation, unless otherwise indicated. Where Shapiro-Wilk tests revealed non-normal data distributions, non-parametric tests were used. Means of data distributions were compared using the Mann-Whitney U test and Wilcoxon test for paired samples. Differences were considered significant where $P < 0.05$ (* $P < 0.05$, ** $P < 0.01$, *** $P < 0.001$, **** $P < 0.0001$). Correlation is given as Pearson Correlation Coefficient (r).

3 Results

3.1 Inhibition of the PPnT facilitates habituation to repeated stimulation of NTSR neurons

To examine the role of the PPnT in collicular-driven stopping behavior, we injected a viral vector for expression of the inhibitory DREADD receptor hM4D (AAV2-hSyn-hM4D(Gi)-mCherry) in the PPnT of NTSR x ChR2 mice (Figure 7A, C). Control animals were injected into the PPnT with an AAV carrying the gene of a yellow-fluorescent protein (YFP) as a reporter. Fiber optic cannulae were implanted over the medial superior colliculus for optogenetic stimulation of ChR2-expressing neurons (Figure 7A-B). Mice were tested in an open field set-up, during which they were allowed to explore freely. Mice tended to actively explore the arena throughout the test, moving between corners and crossing the open space frequently. When the mouse ran across the center of the arena (mean speed 22.1 ± 5.8 cm/s in 0.5 s before stimulation), we manually triggered the laser (blue light, 473 nm), stimulating the colliculus at 20 Hz for 1 second (Figure 7D). All animals underwent five sessions separated by 48 hours with the exception of Session 5, which took place 7 days after Session 4. The hM4D actuator CNO was administered (i.p.) prior to the second session to inhibit the PPnT. Saline was administered prior to all other sessions . Each animal was stimulated approximately 15 times in each 20 minute session (16 ± 2 for hM4D animals, 15 ± 2 for controls). The behavioral profiles and speed dynamics of animals expressing hM4D were compared to those of control animals expressing YFP.

In Session 1 (saline injection), optogenetic stimulation consistently induced a dramatic, invariant speed drop and stopping episode in both groups. The median drop in speed was 97.6% (IQR: [95.4, 98.5]) for hM4D and 97% (IQR: [96.0, 98.3]) for controls, with the comparison made between 0.5 s before stimulation and last 0.5 s of 1 s stimulation period (Figure 7E-G, Video S2). Stopping episodes (defined as speed <1.5 cm/s for > 0.33 s) lasted 1.27 s (median, IQR: [0.7, 1.3]) for hM4D mice and 1.23 s (median, IQR: [0.93, 1.45]) for control mice in Session 1 on average. The median probability of stopping was 1.0 for both the hM4D group and control group (IQR: [1.0, 1.0] and [0.93, 1.0] respectively). Speed during stimulation and probability of stopping did not differ significantly between groups (Mann-Whitney U test; P = 0.352, P = 0.332 respectively, Figure 7I-J).

Upon CNO administration and consequent PPnT inhibition in Session 2, hM4D-expressing mice showed a significantly lower probability of stopping compared to controls (Mann-Whitney U test; P = 0.008; Figure 7J) as well as significantly higher average speeds during stimulation (Mann-Whitney U test; P = 0.013; Figure 7I). Median probability of stopping was 0.65 (IQR: [0.53, 0.79]) for hM4D mice and 0.88 (IQR: [0.84, 0.92]) for controls. Paired samples Wilcoxon tests revealed a highly significant difference in the stopping probability of hM4D-expressing mice in Session 2 (CNO) compared to Session 1 (saline) (P = 0.0004), while control mice showed no significant difference (P = 0.063) (Figure S1C). Stopping probability in Session 2 (CNO) did not correlate to the number of times the mouse was stimulated (r = -0.241; Figure S1D), nor did stopping probability differ significantly between male and female mice expressing hM4D (Mann-Whitney U-test; P = 0.180; Figure S1E).

We found that inhibition of the PPnT increased the variability of the responsiveness of mice to the stimulation (Figure 7E-G). An examination of the evolution of behavior over trials within Session 2 (CNO) revealed that hM4D mice habituated more rapidly to the stimulus than controls, as indicated by a progressive increase in median speed and decrease in percentage of mice stopping during the stimulation (Figure 7H, Video S3). Control mice showed little to no habituation to repeated NTSR collicular stimulation over Session 2 (Video S3).

Over subsequent sessions in which saline was administered, recovery of the attenuated stopping response did not occur (Figure 7J), and hM4D mice tended to exhibit higher median speeds during stimulation than controls (Figure 7I, Figure S1A-B). Taken together, these results suggest that inhibiting the PPnT facilitates habituation to repeated stimulation of collicular NTSR neurons.

3.2 Histological validation and analysis of relationship to stopping probability

To validate our behavioral results, we performed histological analysis of fiber placement and viral expression in sectioned brains and examined the relationship between stopping behavior and the location of viral expression. Fiber tip placement was -3.4 ± 0.3 mm from Bregma on the AP plane for hM4D mice (Figure S2), and -3.3 ± 0.3 mm for YFP controls (Figure S4B). All animals stopped consistently during the first session, indicating that NTSR neurons were stimulated in all cases. ChR2 expression in NTSR x ChR2 crossed mice was confirmed with confocal microscopy (Figure 7B). Viral expression of hM4D/YFP in the PPnT, indicated by mCherry/YFP fluorescence, was also verified histologically (Figure 8A-B, Figure S3A, Figure S4A). Alignment with the Allen Mouse Brain Atlas showed the following variability in the coordinates of the center of hM4D expression: AP -3.15 mm ± 0.2, ML 1.8 mm ± 0.1, DV 3.4 mm ± 0.1 (Figure 8A-C). AP spread of the virus was 0.64 mm ± 0.14 (Figure 8D). Viral expression in the PPnT was confirmed in all cases and all animals were included in behavioral analysis (n=24).

To investigate the relationship between stopping behavior and the specific location of hM4D expression in the PPnT, we examined the correlation between stopping probability in Session 2 (CNO) and the coordinates of the center of expression (Figure 8C) as well as the anteroposterior spread of expression (Figure 8D). Linear regression revealed no correlation with coordinates on the AP, ML, and DV planes or the extent of expression (Pearson coefficient r = 0.112, 0.245, -0.293 and -0.297 respectively). Additionally, we compared the stopping probability of animals with and without hM4D expression in the specific nuclei of the PPnT (Figure 8E). All mice had expression in the POL. PoT expression was present in most animals (n=13/17), but its presence or absence had no effect on stopping probability (Mann-Whitney U-test; P = 0.198). Expression in the PIL and SGN was observed in approximately 50% of the animals (PIL: n=9/17; SGN: n=8/17). Interestingly, rather than causing the behavioral attenuation, expression in these areas seemed to interfere with the effect, increasing stopping probability (Mann-Whitney U-test; PIL: P = 0.037; SGN: P = 0.042). Viral expression in the caudal LP was observed in several animals (n=8/17), but this had no effect on stopping probability (Mann-Whitney U-test; P = 0.168, Figure 8F). Expression in the dentate gyrus (DG) and motor layers of the SC (SCm) also had no effect on stopping probability (P = 0.500 and 0.405 respectively, Figure S3B). Overall, animals with the greatest attenuation of

stopping behavior exhibited expression centered in the POL, suggesting that inhibition of this area facilitates habituation to repeated activation of collicular NTSR neurons.

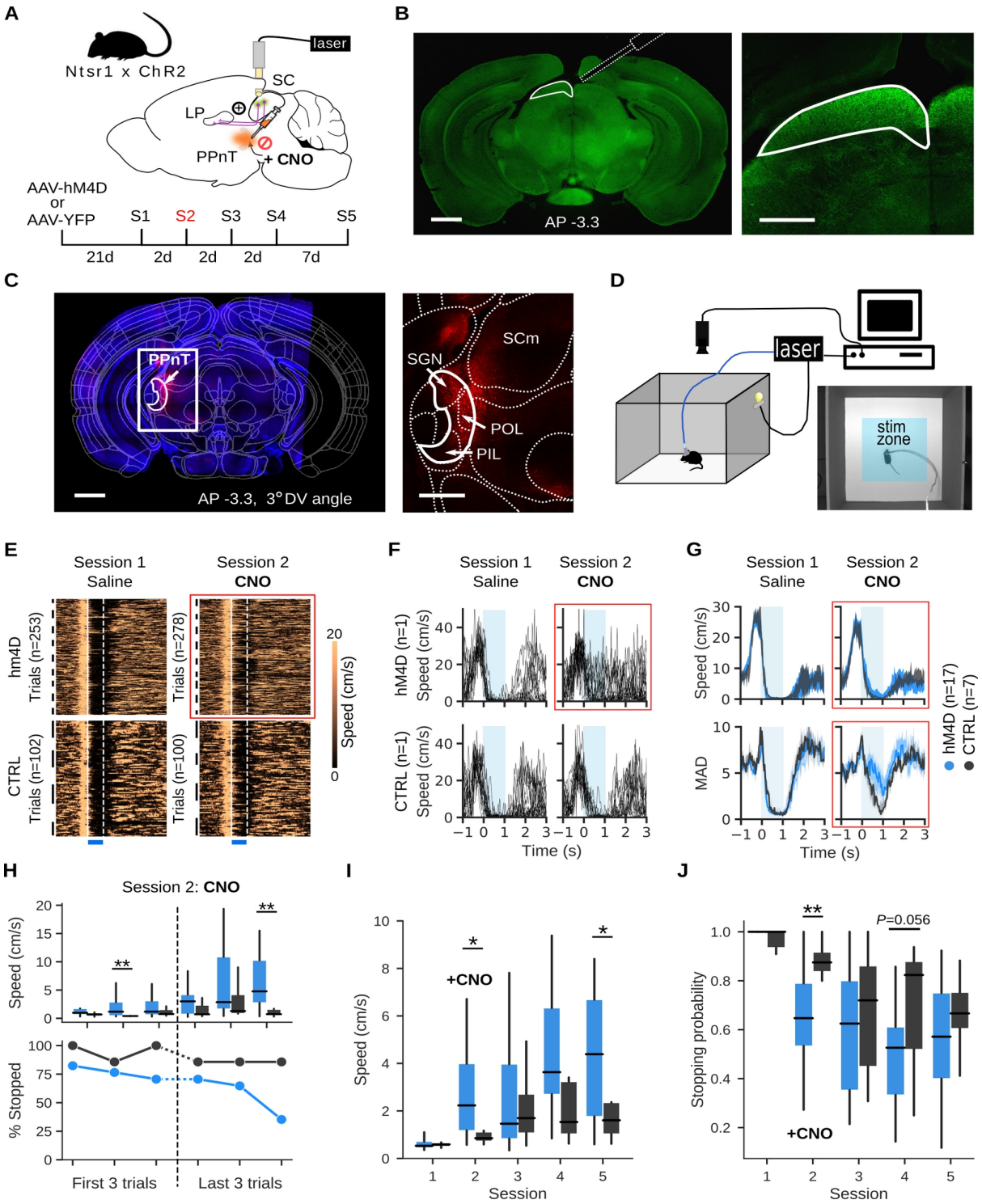

FIGURE 7 | PPnT inhibition facilitates habituation to stimulation of NTSR collicular neurons. A. Experimental paradigm. **B.** Coronal sections showing fiber implantation (left) and ChR2 expression (right) in NTSR x ChR2 mouse for optogenetic stimulation of the medical retinorecipient layers of the colliculus. Fiber is delineated by dotted white lines, and superfical layers of the superior colliculus are outlined in solid white. Scale bar, 1 mm (left), 500 µm

(right). **C.** Confocal image of coronal section aligned to the Allen Mouse Brain Atlas showing AAV2-hSyn-hM4D(Gi)-mCherry expression (red) in the PPnT (outlined in solid white) of NTSR x ChR2 mouse. White box (left) indicates area of enlargement (right) with demarcation of PPnT areas SGN, POL, and PIL. Scale bar, 1 mm (left), 500 µm (right). **D.** Open field set-up for optogenetic stimulation. **E-G.** Red box indicates plots where PPnT is inhibited in hM4D mice. **E.** Heatmaps showing speed over time for NTSR x Chr2 AAV-hM4D mice (top row, n=17) and AAV-YFP controls (bottom row, n=7) over first two sessions. Each row in the heatmap is a single trial, and trials belonging to a single animal are indicated by the vertical black lines on the left of the plot (hMD4 trials per mouse, Session 1 = 15 ± 2, Session 2 = 16 ± 3; CTRL trials per mouse , Session 1 = 15 ± 2, Session 2 = 14 ± 2). Blue rectangle (bottom) indicates when laser was on, and vertical white lines show stimulus onset and offset. **F.** Speed traces from Session 1 (left) and Session 2 (right) for all trials of one hM4D mouse (top row) and one control mouse (bottom row). Blue shaded rectangle indicates stimulation (0 to 1 s). **G.** Top row, median speed over time of all hM4D (blue) and control (gray) mice for all trials of Session 1 and 2. Bottom row, mean absolute deviation (MAD) in speeds across trials for hM4D (blue) and CTRL (gray) animals. **H.** Median speed during stimulation (top row) and percentage of mice that stopped (bottow row) during first and last 3 trials of Session 2 for hM4D (blue) and CTRL (gray) mice. **I.** Overview of median speed during stimulation for all five sessions for hM4D (blue) and CTRL (gray) mice. **J.** Overview of stopping probability across trials for all five sessions for hM4D (blue) and CTRL (gray) mice. Box and whisker plots indicate median, IQR, and range of distribution. Significance was tested using Mann-Whitney U-test (alpha = 0.05). * $P < 0.05$, ** $P < 0.01$.

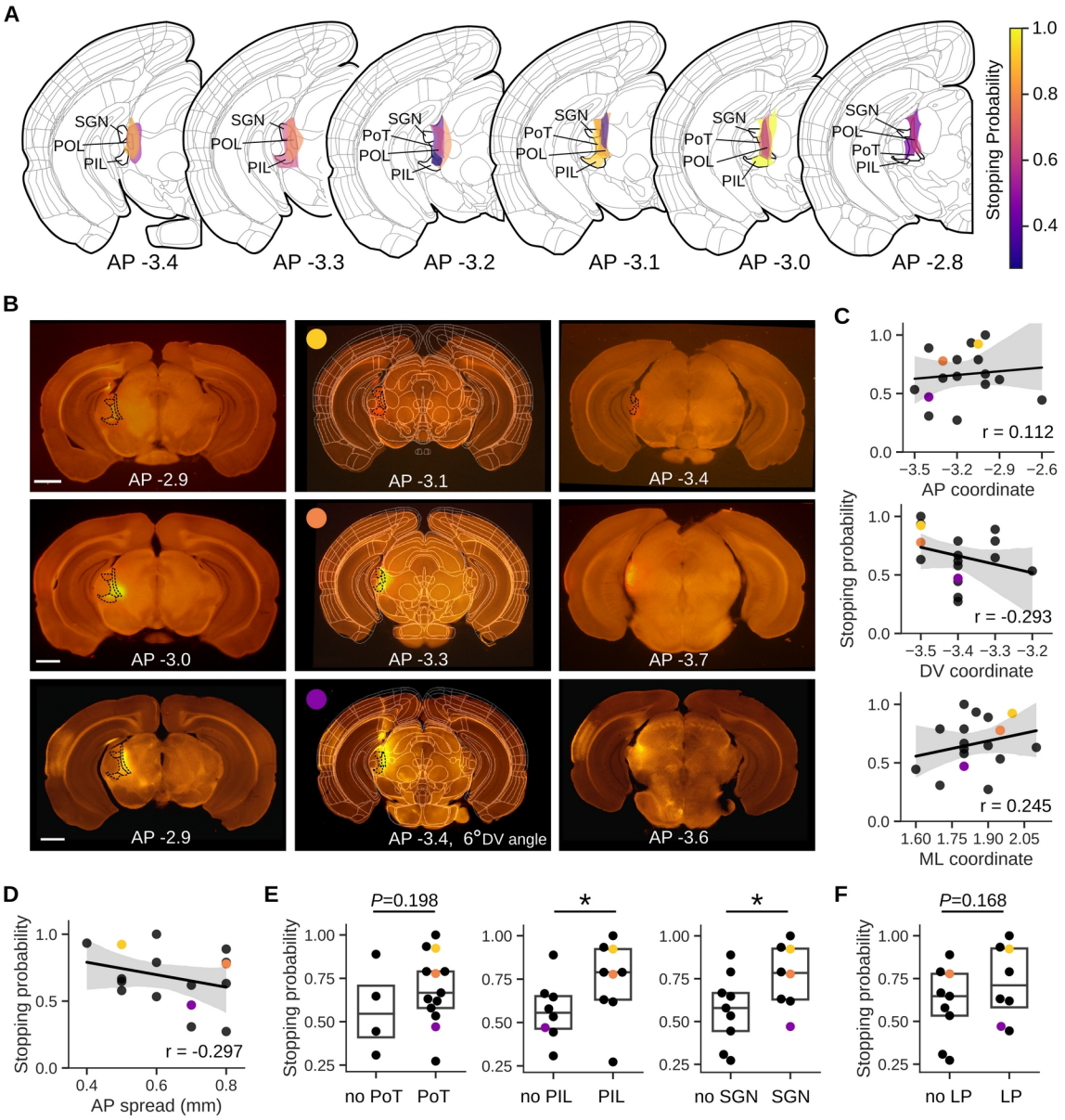

FIGURE 8 | Histological analysis of AAV-hM4D expression in the PPnT.
A. Schematic representation of the centers of AAV-hM4D expression for all animals (n=17) grouped on the AP plane. Color represents stopping probability in the CNO-administered session. PPnT areas are outlined and labeled in black. **B.** Coronal sections from three example brains aligned to the Allen Mouse Brain Atlas. Each row contains images from a single animal, and in each column is an image of the anterior limit of hM4D expression (left), center of expression (center), and posterior limit of expression (right). The PPnT areas, where present, are outlined by dashed black lines. Colored circle in the center column indicates stopping probability of the associated animal based on the colormap in Panel A. Scale bar, 1 mm. **C-F.** Colored points correspond to histology examples given in Panel B. **C.** Relationship of Session 2 (CNO) stopping probability of AAV-hM4D mice to injection center coordinates on the AP (top), DV (center), and ML (bottom) planes (n=17). Black line is line of best-fit from linear regression, and shaded area represents the 95% confidence interval. **D.** Relationship of Session 2 (CNO) stopping probability to AAV-hM4D anteroposterior spread of expression. **E.** Stopping probability of AAV-hM4D mice with and without expression in the PoT (left), PIL (center), and SGN (right). **F.** Stopping probability of AAV-hM4D mice with and without expression in the LP. Box plots indicate median and IQR. Significance was tested using Mann-Whitney U-test (alpha = 0.05). * $P < 0.05$.

3.3 Stimulation of wide-field neurons is sufficient to elicit stopping behavior

As NTSR x ChR2 mice express ChR2 in all NTSR-positive cells, we performed a control experiment to verify that stimulation of a targeted population of wide-field neurons alone is sufficient to induce stopping behavior. To test this, we delivered a targeted injection of AAV-DIO-ChR2 to the medial retinorecipient layers in the colliculus of NTSR1-Cre mice (n=16) (Figure 9A). In a behavioral paradigm identical to that described above, 4 out of 16 mice stopped consistently upon optogenetic stimulation. Histological analysis confirmed that mice with little or no ChR2 expression in the SC, or a mismatch between the injection site and fiber placement did not respond to the stimulation, and these mice were removed from further analysis (n=12, Figure S5C).

For mice with ChR2 expression aligned correctly with the fiber tip (n=4; Fig 9B, Figure S5B), optogenetic stimulation of the superior colliculus evoked consistent stopping behavior in Session 1 when compared with Cre-negative NTSR x ChR2 controls (n=8; Fig 9C-D, Video S4). NTSR1-Cre animals showed significantly lower speeds during stimulation ($P < 0.0001$; Fig 9E) and greater stopping probability ($P = 0.007$; Fig 9F) than controls. These results suggest that stimulation of wide-field neurons is sufficient to elicit stopping behavior, indicating that optogentically-induced stopping behavior in NTSR x ChR2 mice is not due to nonspecific activation of axon terminals or fibers of passage.

3.4 NTSR1-Cre mice display behavioral trends comparable to NTSR x ChR2 mice upon PPnT inhibition

To test the behavioral effect of PPnT inhibition when stimulating a targeted wide-field neuron population, ChR2-expressing NTSR1-Cre mice were injected with hM4D into the PPnT and underwent 5 sessions of behavioral testing identical to NTSR x ChR2 mice (Figure 10A). hM4D expression in the PPnT was verified in each animal (Figure 10B, Figure S5A).

While the speed of hM4D NTSR1-Cre animals compared to hM4D NTSR x ChR2 during stimulation was higher over sessions (Figure 10C-D), both groups exhibited a comparable trend of speed increase upon CNO administration in Session 2 compared to Session 1 (saline), which was not observed in YFP-expressing NTSR x ChR2 controls (Figure 10E, Video S5). Analysis of the fold change in speed from Session 1 to Session 2 revealed that hM4D NTSR x ChR2 mice did not differ from hM4D NTSR1-Cre mice ($P = 0.280$), while both groups differed significantly from control animals ($P = 0.007$ for hM4D NTSR x ChR2 and $P = 0.024$ for hM4D NTSR1-Cre, Figure 10F).

Stopping probability of NTSR1-Cre mice, while initially lower than NTSR x ChR2 mice, mirrored the pattern of decrease in hM4D NTSR x ChR2 mice (Figure 10G). The difference in stopping probability between Session 1 and Session 2 did not differ significantly between NTSR1-Cre and NTSR x ChR2 hM4D animals ($P = 0.131$), while both groups differed from control animals ($P = 0.005$ and 0.009 for NTSR1-Cre and NTSR x ChR2 hM4D mice respectively; Figure 10H). These results support the finding that inhibition of the PPnT facilitates habituation to repeated stimulation of wide-field neurons.

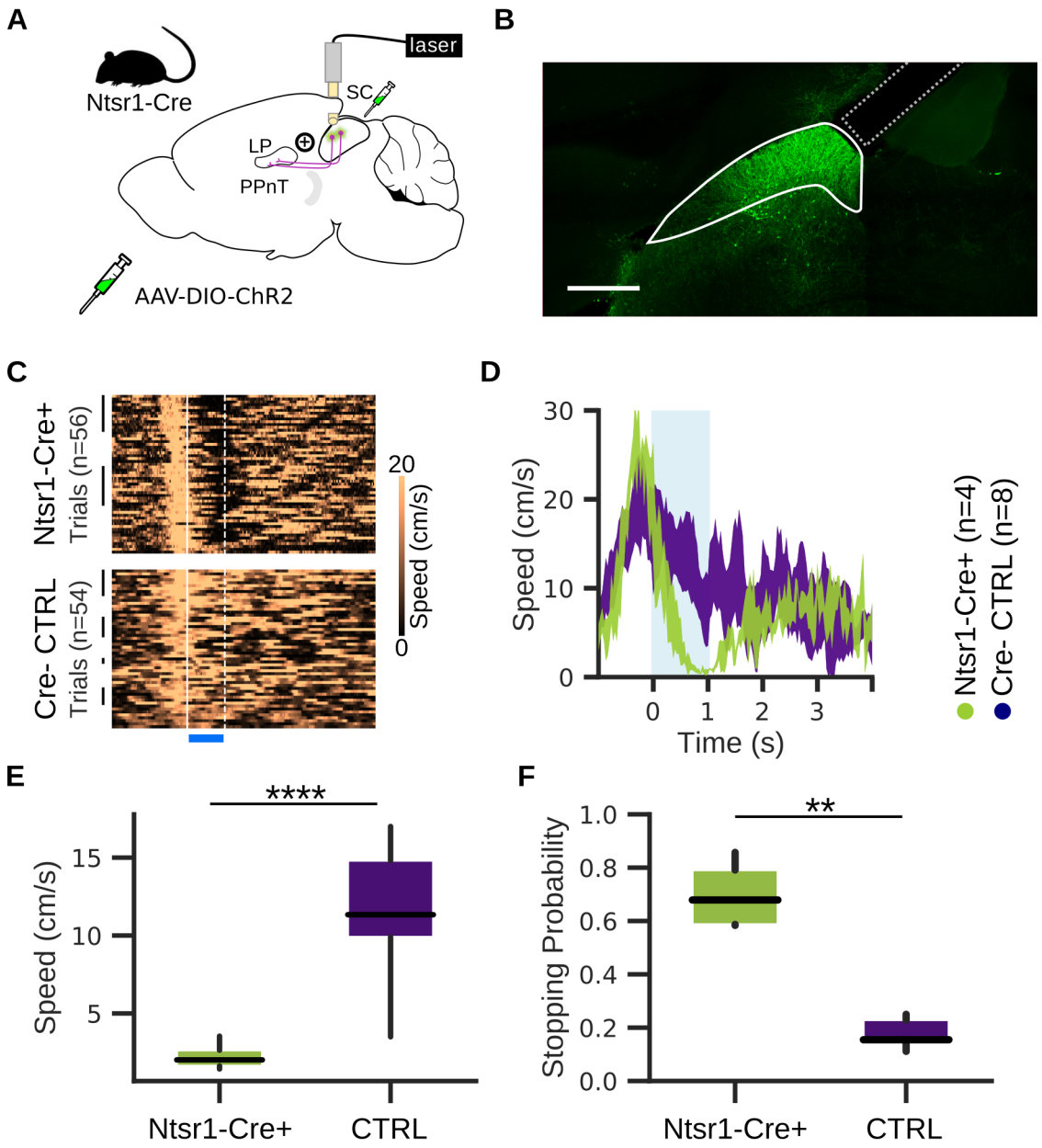

FIGURE 9 | Stimulation of wide-field neurons is sufficient to elicit stopping behavior. A. Scheme of injection strategy for NTSR1-Cre mice. **B.** Confocal image of coronal section showing the fiber tip (dotted line) aligned with ChR2 expression in the retinorecipient layers of the superior colliculus (outlined with solid white line) in NTSR1-Cre mouse. Scale bar, 500 µm. **C.** Heatmaps showing speed over time for NTSR1-Cre+ mice and Cre-negative controls. Each row is a single trial, and trials belonging to a single animal are indicated by the vertical black lines. Vertical white lines show stimulus onset and offset. **D.** Median speeds over time of NTSR1-Cre+ (green) and Cre-negative control (indigo) mice. Stimulus onset and offset (0 to 1 sec) delineated by blue rectangle. **E.** Comparison of speed during stimulation for NTSR1-Cre+ (green) and control mice (indigo). **F.** Comparison of stopping probability for NTSR1-Cre+ (green) and control mice (indigo). Box and whisker plots indicate median, IQR, and range of distribution. Significance was tested using Mann-Whitney U-test (alpha = 0.05). ** $P < 0.01$, **** $P < 0.0001$.

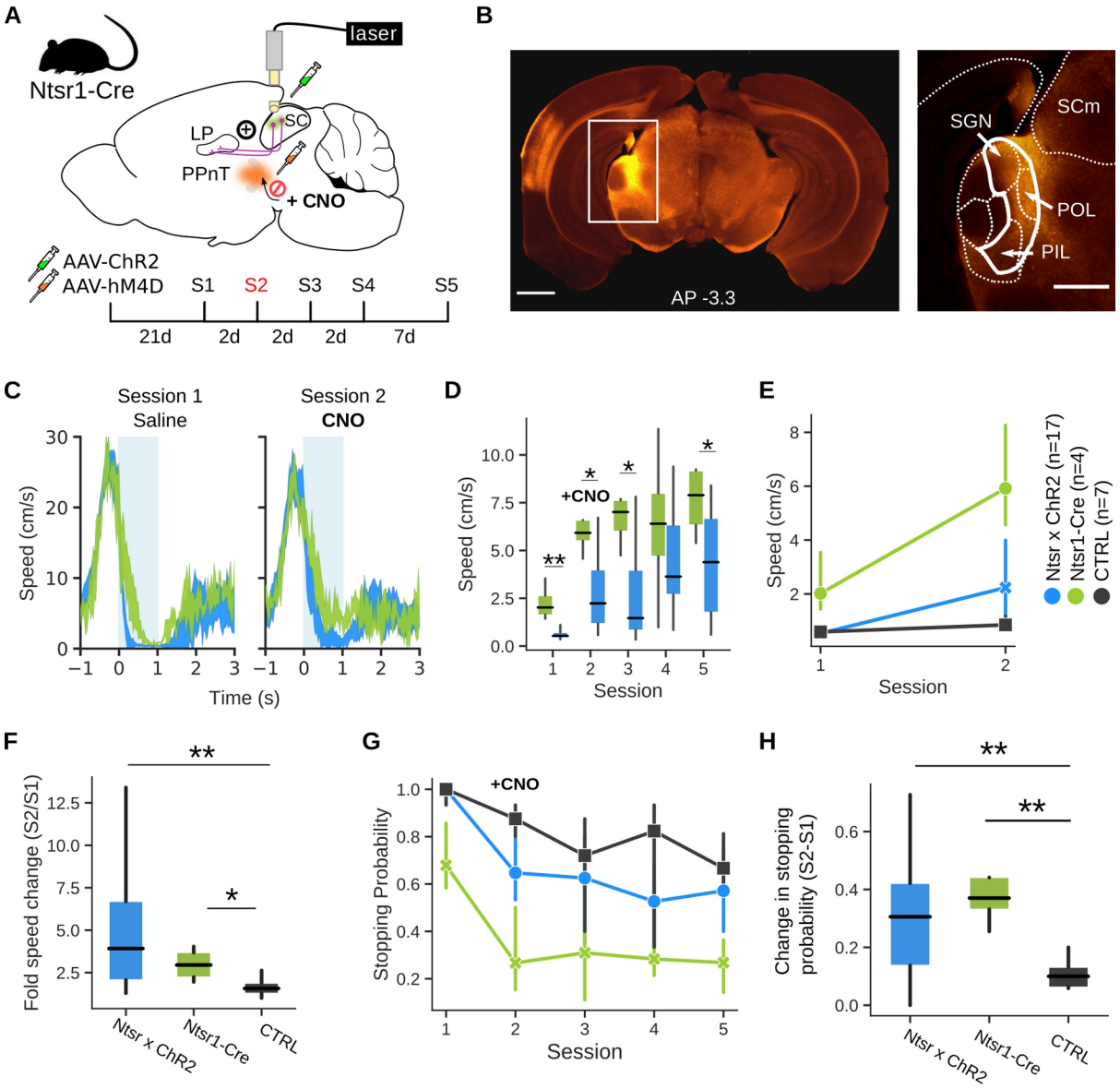

FIGURE 10 | NTSR1-Cre display behavioral trends comparable to NTSR x ChR2 mice upon PPnT inhibition. A. Scheme of injection strategy and behavioral testing for NTSR1-Cre mice. **B.** Coronal slice (left) showing expression of AAV-hSyn-hM4D(Gi)-mCherry in the PPnT of NTSR1-Cre mouse. White rectangle shows area enlarged in right panel. PPnT is outlined in solid white (right), and the specific areas in the PPnT (POL, SGN, and PIL) are outlined in dashed white lines. Scale bar, 1 mm (left), 500 µm (right). **C.** Overlay of median speeds for Session 1 and 2 for hM4D NTSR1-Cre (green) and hM4D NTSR x ChR2 (blue) mice. Stimulus onset and offest (0 to 1 sec.) delineated by blue rectangle. **D.** Median speed during stimulation for all five sessions for NTSR1-Cre (green) and NTSR x ChR2 mice (blue). **E.** Comparison of median speed during stimulation for hM4D NTSR1-Cre (green), hM4D NTSR x ChR2 (blue), and YFP control (gray) groups during first two sessions. Error bars represent 95% confidence interval. **F.** Fold change in speed from Session 1 to Session 2 in all groups. **G.** Stopping probability over all sessions, for all groups. Error bars represent 95% confidence interval. **H.** Difference in stopping probability between first two sessions for all groups. Box plots indicate median, interquartile range, and range of the distribution. Significance was tested using Mann-Whitney U-test (alpha = 0.05). $*P < 0.05$; $**P < 0.01$.

3.5 Retrograde viral tracing suggests inputs to the PPnT arrive from across the midbrain and select areas in the limbic system and cortex

To determine inputs to the PPnT in mice, we injected 200 nl HSV-Cre, a retrograde viral tracer, into the PPnT of a tdTomato mouse (n=1) (Figure 11A). Subsequent histological analysis and confocal imaging revealed a variety of labeled areas across the midbrain, limbic system, and cortex (Figure 11B-C). In the midbrain, dense labeling was observed in the superior colliculus, inferior colliculus, cuneiform nucleus, PAG, and precommissural nucleus. Within the superior colliculus, most labeled cell bodies were in the superficial layers, with the greatest density in the optic layer and the lateral portion of the superficial gray layer. Sparser labeling was present in the motor layers of the colliculus. Inferior collicular expression was greatest in the external nucleus, and labeling in the PAG was greatest in the dorsal and dorsolateral portion. Less dense labeling was observed in the PBG and parabrachial nucleus. In the limbic system, labeled cells were found in the amygdala (central and medial nuclei), hypothalamus (tuberal nucleus and ventromedial nucleus), and zona incerta. Labeled cortical areas included the VISpor, somatosensory cortex (supplementary and primary areas, layer 5 and 6a), auditory cortex (layer 6a), with sparse labeling in the motor cortex. Widespread labeling in thalamic regions adjacent to the injection site was also noted. Sparse labeling was also observed throughout the pons and medulla, with concentrations in the nucleus prepositus and spinal trigeminal nucleus**.**

Anecdotal observation of the axon terminals of m-Cherry-stained neurons from the PPnT of a mouse in behavioral experiments (n=1) revealed expression in the cortex, midbrain, and limbic system (Figure S6). Cortical labeling was seen in the retrosplenial area, posterior and ventral auditory areas, temporal association areas, and ectorhinal area (Figure S6A). In the limbic system, the midline thalamic complex, reticular nucleus of the thalamus, lateral amygdala, and zona incerta were labeled (Figure S6C-D). Midbrain expression was observed in the cuneiform nucleus, inferior colliculus, superficial layers of the superior colliculus, and dorsolateral PAG (Figure S6B), highlighting these areas as possible targets of the PPnT. This anecdotal evidence give a first approximation of the inputs and outputs of the PPnT in mice and opens the door to a thorough examination of nucleus-specific circuitry and the precise involvement in visually guided defensive behavior.

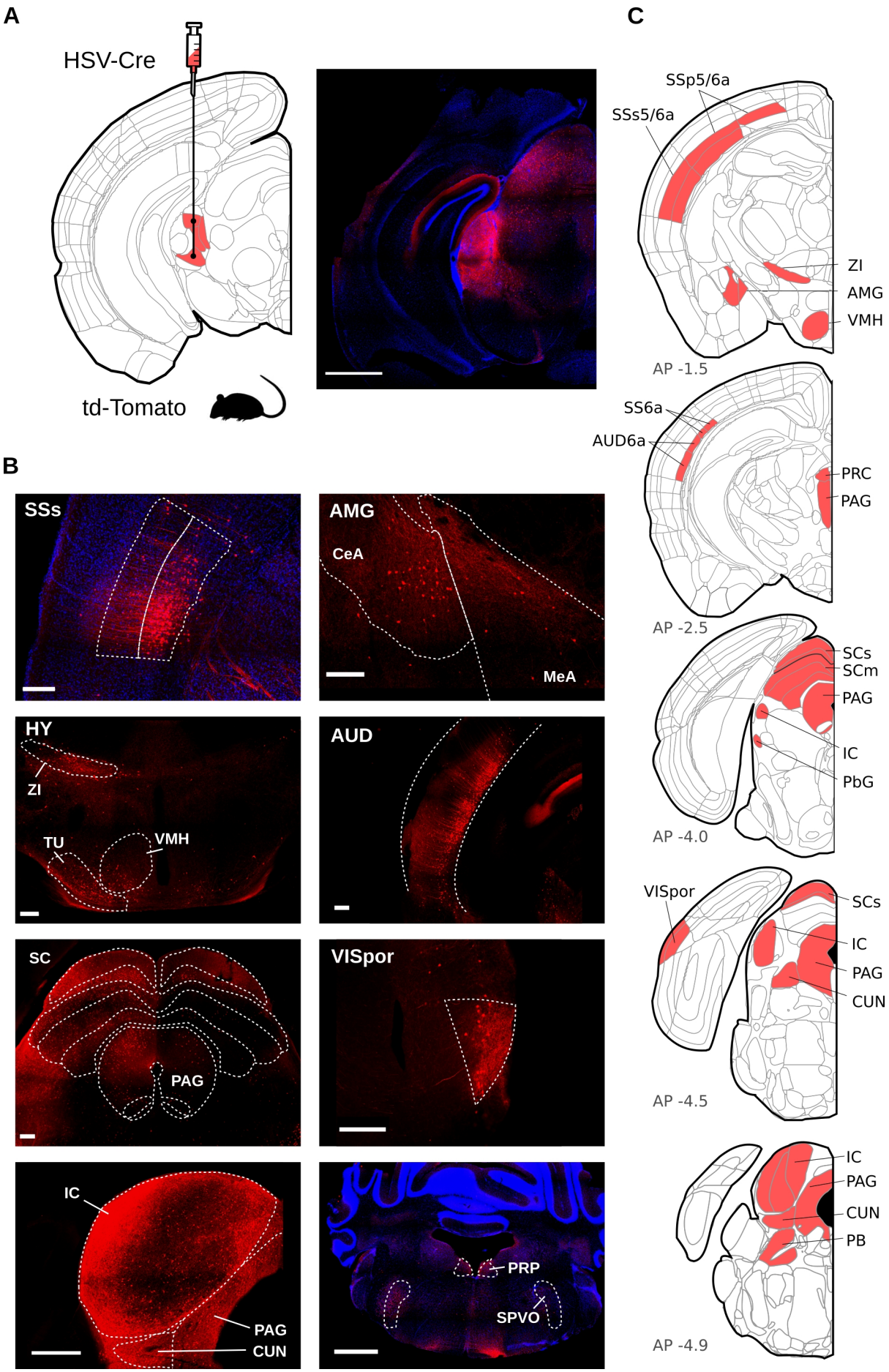
A
HSV-Cre
td-Tomato
B
SSs
AMG
CeA
MeA
HY
ZI
TU
VMH
AUD
SC
PAG
VISpor
IC
PAG
CUN
PRP
SPVO
C
SSp5/6a
SSs5/6a
ZI
AMG
VMH
AP -1.5
SS6a
AUD6a
PRC
PAG
AP -2.5
SCs
SCm
PAG
IC
PbG
AP -4.0
VISpor
SCs
IC
PAG
CUN
AP -4.5
IC
PAG
CUN
PB
AP -4.9

FIGURE 11 | Retrograde viral tracing reveals inputs to the PPnT. A. Injection of Cre-dependent HSV virus into PPnT of tdTomato mouse (left). Confocal image (right) shows td-Tomato expression at injection site (AP -3.2). Scale bar, 1 mm. **B.** Confocal images of selected regions with the highest amounts of tdTomato labeling. Blue shows DAPI staining. All unilateral images are ipsilateral to the injection site, with the exception of the VISpor, which showed labeled cells contralaterally. Scale bar (bottom right image), 1 mm. Scale bar, (all others) 200 μm. SSs somatosensory cortex, supplementary, AMG amygdala, CeA central nucleus amygdala, MeA medial nucleus amygdala, HY hypothalamus, ZI zona incerta, TU tuberal nucleus, VMH ventromedial nucleus hypothalamus, AUD auditory cortex, SC superior colliculus, PAG periaqueductal gray, VISpor visual postrhinal cortex, IC inferior colliculus, CUN cuneiform nucleus., PRP prepositus nucleus, SPVO spinal nucleus trigeminal, oral. **C.** Summary of suggested inputs to the PPnT. SSp somatosensory cortex, primary, PRC precommissural nucleus, SCs superior colliculus, superficial layers, SCm superior colliculus, motor related, PBG parabigeminal nucleus, PB parabrachial nucleus.

4 Discussion

Innate defensive behaviors are highly complex, as they involve the integration of sensory information to influence motor output automatically. The underlying circuits then, require tortuous projections connecting areas dispersed across the brain. When it comes to collicular-driven behaviors, very few specifics are known about how functional nodes downstream from the colliculus contribute to and mediate behavioral output. The PPnT have been linked to fear conditioned responses, but have never been implicated in the wide-field neuron collicular circuit nor in innate defensive behaviors in mice in general. We give a first approximation of the role of the PPnT in innate behaviors, by examining this collicular circuit specifically. Our study of the PPnT reinforces the power of functional whole brain imaging to identify novel areas associated with specific behaviors and then manipulate them directly. We show that directly manipulating these functional nodes can uncover novel roles for brain regions. These types of studies are vital for a thorough understanding of neural circuits. Dissecting the specific cell-types, projections and nuclei involved in innate behaviors in a rodent model is necessary to begin to understand how dysregulation of homologous circuits in humans can lead to phobias, post-traumatic stress, and anxiety disorders.

4.1 A novel role for the PPnT in mediating innate collicular-driven behavior

To investigate the role of the PPnT in collicular-driven behavior, we simultaneously stimulated NTSR neurons in the colliculus with optogenetics while chemogenetically silencing the PPnT using the inhibitory DREADD hM4D in a transgenic mouse model. We discovered that inhibition of the PPnT resulted in quicker habituation to repeated optogenetic stimulation of NTSR neurons. hM4D-expressing mice who exhibited stereotyped and consistent stopping behavior upon collicular stimulation in saline trials, habituated quickly to the stimulation upon administration of the actuator CNO, resulting in an attenuated stopping response compared to controls. Our results suggest a novel role for the PPnT in this circuit, which can be linked to previous work showing the PPnT to have a function in multimodal sensory, striatal, and limbic systems.

4.2 Evidence of afferent and efferent projections of the PPnT

To our knowledge, we provide novel evidence here for afferent connections of the PPnT in the mouse using retrograde viral tracing in a reporter mouse line. Our results suggest that inputs to this group of nuclei arrive from across the cortex, midbrain, and limbic system with labeled regions exhibiting high correspondence to inputs identified in rat tracing studies. To get an indication of efferent projections from the PPnT, we examined mCherry-labeled axon terminals from the PPnT in mice in the behavior study and found labeling across the cortex, limbic system, and midbrain as well. Here, we first position our tracing study in the context of previous literature and then discuss how these pathways correlate to putative functions of the PPnT.

4.2.1 Afferent connections

Projections to the PPnT are foremost described to originate from multiple sensory systems, namely the visual, auditory, and somatosensory systems with inputs arriving from the superior colliculus (Linke, 1999; Hicks et al., 1986; Tanaka et al., 1985), the external cortex of the inferior colliculus (Linke, 1999; LeDoux et al., 1985; Yasui et al., 1990), spinal trigeminal nucleus (Peschanski, 1984), and across the temporal association, auditory, and insular cortex (Linke and Schwegler, 2000; Hicks et al., 1986; Yasui et al., 1990). Within the superior colliculus, optic and intermediate layers project to the SGN in the rat and cat, while deep layers project to the rat PIL (Linke, 1999; Hicks et al., 1986; Tanaka et al., 1985). Projections to the PAG have been observed in the rat and cat (Kincheski et al., 2012; Hicks et al., 1986), and retrograde labeling also revealed afferent connections in the ZI, VMH, and pontine reticular nucleus in the cat (Hicks et al., 1986). In our study in the mouse, we observed labeling in the superior colliculus, inferior colliculus, spinal trigeminal nucleus, auditory cortex, ZI, VMH, and across the pons (Figure 11). As our results are highly consistent with literature on rats and cats, these afferent projections are likely valid in mice

Many of these regions are widely associated with innate defensive behavior, securing a place for the PPnT in the discussion of innate behavior in mice. For example, a host of literature describes the dorsolateral PAG (dlPAG) as playing a fundamental role in risk assessment and mediation of flight and freezing behaviors (Deng et al., 2016; Assareh et al., 2016; Vianna and Brandão, 2003; Bittencourt et al., 2004). It has been suggested that fear learning due to dlPAG stimulation in rats is mediated in part by its outputs to the SGN and subparafascicular nucleus of the thalamus (SPF), a region adjacent to the PPnT (Kincheski et al., 2012; Silva et al., 2016). The hypothalamus has recently become a focus in innately-driven behavior, and optogenetic stimulation of the VMH induces flight and freezing in a circuit that bypasses the amygdala (Kunwar et al., 2015). In terms of sensory input, stimulation of the projection from the auditory cortex to the inferior colliculus causes freezing (Xiong et al., 2015), and auditory-induced flight is facilitated by somatosensory input in mice, which is mediated by a projection of PV+ cells from the ZI to the thalamus (Wang et al., 2019). The integration of sensory modalities can influence behavioral output, and the PPnT circuit in question could be a prime example of that.

4.2.2 Efferent connections

Efferent pathways from the PPnT are known to target the limbic system, basal ganglia, midbrain, and cortex in the rat. Within the limbic system, projections have been recorded in the lateral, basomedial, and medial portion of the central amygdalar nuclei as well as the VMH (Namura et al., 1997; Linke et al., 2000; LeDoux et al., 1984; LeDoux et al., 1985). In the basal ganglia, the tail of the CPu and the globus pallidus receive PPnT projections (Moriizumi and Hattori, 1992; Shammah-Lagnado et al., 1996; LeDoux et al., 1985; Arnault and Roger, 1990). Midbrain targets include the external cortex of the inferior colliculus (Senatorov and Hu, 2002; Winer et al., 2002; Arnault and Roger, 1990), deep superior colliculus and PAG (Arnault and Roger, 1990). In the cortex, projections from the PPnT target the temporal cortical areas (Namura et al., 1997; Arnault and Roger, 1990). In the mouse, tracing studies have identified the lateral amygdala and auditory cortex as outputs of the PPnT and adjacent medial portion of the medial geniculate complex (MGm; Keifer et al., 2015; Asede et al., 2015). Hypothalamus, CPu and midbrain projections are also noted in a general sense (Keifer et

al., 2015). Our observations are consistent with these prior studies. We noted labeling in the following corresponding regions: auditory and temporal association areas, lateral amygdala, inferior colliculus, superior colliculus, and dlPAG (Figure S6).

It is of interest that there is considerable overlap between regions identified by retrograde and anterograde analysis. This suggests some reciprocal connections, such as the SGN-superior colliculus bilateral reciprocal connection previously described (Tanaka et al., 1985). As discussed above, many of these brain regions are considered imperative to the innate threat response system of rodents. Of note, in our study the retrosplenial cortex and temporal association areas were uniquely observed in the anterograde direction. The retrosplenial and anterior cingulate cortical areas are thought to play a role in contextual fear learning (LeDoux, 2000; Maren, 2011; Maren, 2001) and innate defensive behaviors (Jhang et al., 2018; Mongeau et al., 2003; Silva et al., 2016). The PPnT appears to be in an ideal position to combine information from sensory modalities and prior risk assessment to influence future decisions.

4.2.3 Where does the PPnT fit into the NTSR collicular circuit?

How do signals reach the PPnT from the LP? How does the PPnT integrate information from multiple sensory systems to influence and update motor output? These details remain unclear. However, based on our tracing results, which are supported by established research, we explore several possibilities. We know that wide-field neurons directly course from the superficial superior colliculus to the LP. The PPnT is also known to receive input from the superior colliculus in the rat and cat, and we observed retrograde labeling here as well. Thus, it is possible that there are local interactions between wide-field neurons and other sub-populations of cell types in the optic layer of the colliculus. Previous literature argues that NTSR collaterals do not exist within the colliculus, so this possibility is unlikely (Gale and Murphy, 2018). This would, however, be the fastest, direct pathway for NTSR neurons to interact with the PPnT and cannot yet be ruled out entirely.

We can also consider a place for the PPnT downstream from the LP and its immediate outputs. The LP provides direct output to the VISpor, and our tracing results suggest that the PPnT receives inputs from the VISpor. We also observed retrograde labeling in the central amygdala, suggesting efferent projections from this region to the PPnT. The central amygdala receives projections from the lateral amygdala, which receives outputs directly from the LP (Wei et al., 2015). The central amygdala is thought to play a role in mediating freezing behavior (Keifer et al., 2015a; LeDoux, 2000). Thus, a SC-LP-VISpor-PPnT or SC-LP-LA-CeA-PPnT circuit is a very viable possibility.

The amygdala is known to project to the hypothalamus and PAG (Roseberry and Kreitzer, 2017; Silva et al., 2016), and we observed retrograde labeling from the PPnT in both the hypothalamus and PAG. Due to dense retrograde labeling in the PAG in our study, we also suggest the possibility of a SC-LP-AMY-PAG-PPnT-SC pathway. The PAG has been proposed to act as a decision-maker based on integration of all the signals it receives and an overall risk assessment (Deng et al., 2016). It is not implausible that information about the decision travels back to the thalamus, to the PPnT, to update information for future decisions. Information from the PAG could then combine with sensory input to the PPnT. The PPnT could act as a sort of regulatory loop in this sense, projecting back to the major sensory systems and updating them based on the information received. In the case of the collicular circuit at hand, we suggest that the

PPnT acts as an intermediary relay to superior colliculus, transmitting updated, relevant information about a stimulus and thereby modifying collicular output.

4.3 Putative roles of the PPnT

The correspondence between tracing studies in the rat and cat and our present results suggests functional homology as well, and we explore the putative roles of the PPnT in the sensory, limbic, and striatal systems below.

4.3.1 Role in binding polymodal stimuli

Consistent with its multimodal sensory inputs and outputs, the PPnT are considered to have a polymodal function as a whole (Wepsic, 1966). Interestingly, previous work has shown that some subsets of neurons within the nuclei can be activated by a single modality of input (visual, auditory, or somatosensory; Linke, 1999; Linke et al., 2000; Hicks et al., 1986; Hicks et al., 1984; Benedek et al., 1997; Bordi and LeDoux, 1994; Bordi and LeDoux, 1994). Neurons in the SGN show visual response properties in cats (Hicks et al., 1984; Krupa et al., 1984), and populations with auditory and somatosensory responses were found in the MGm, PIL, and SGN in single-unit recordings (Bordi and LeDoux, 1994; Bordi and LeDoux, 1994). The lateral portion of the SPF is thought to receive converging auditory and nociceptive inputs (Coolen et al., 2003). Direct involvement of the PPnT in feedback regulation of incoming acoustic signals has been suggested based on evidence of a direct reciprocal connection between the inferior colliculus and PPnT (Senatorov and Hu, 2002).

Based on its inputs from multiple modalities, it follows that the PPnT could play a role in binding of sensory information. Thalamocortical cells in the medial geniculate and PPnT are thought to engage multiple cortical areas at once to integrate sensory information (Jones, 1998; Jones, 1998). These nuclei also activate high-frequency 40 Hz gamma oscillations in the auditory cortex (Barth and MacDonald, 1996; Sukov and Barth, 2001) which are thought to be required for temporal binding of sensory stimuli. The suggested purpose of this sensory integration in the PPnT is to provide input to the amygdala (Linke et al., 1999; Linke et al., 2000).

4.3.2 Role in emotional arousal and conditioned learning

Study of the amygdalar projection from the PPnT provides evidence for its role in emotional arousal and conditioned responses. This projection is thought to induce quick arousal and attention due to emotional events (Wilhelmi et al., 2001). Lesions to the PPnT as well as selective destruction of PPnT-innervated neurons in the central and lateral amygdala in rats blocked conditioned responses to acoustic stimuli (LeDoux et al., 1984; Iwata et al., 1986). As further support for the PPnT's role in learning, some cells within the PPnT possess the SK type calcium-activated potassium channel, which has been implicated in long-term potentiation in the cortex (Ryugo and Weinberger, 1978; Gerren and Weinberger, 1983; McEchron et al., 1996). The PPnT thus appear to be in a position to activate the amygdala and thereby influence the flow of information from cortex to amygdala.

4.3.3 Role in sensory-guided decision making

The PPnT projection to the striatum has been implicated in sensory-guided, reward-driven decision making (Hunnicutt et al., 2016; Arnault and Roger, 1987; LeDoux et al., 1991; Doron and Ledoux, 1999; Guo et al., 2018). Generally speaking, the striatum has been linked to visual selection and attention, as well as visuomotor and auditory processes (Basso and May, 2017; Krauzlis et al., 2014; McHaffie et al., 2006). It has been suggested that action termination following goal completion is mediated by the basal ganglia (Roseberry and Kreitzer, 2017). Recently, the striatal projection from the PPnT was suggested to act as a gain controller and to convey information about the timing of acoustic events (Ponvert and Jaramillo, 2019; Chen et al., 2019). It is particularly interesting that downstream activity was also identified in the tail of the CPu in fUSi recordings during NTSR collicular stimluation. This region's precise contribution to the collicular stopping behavior remains to be explored.

4.3.4 Suggested role in prevention of behavioral adaptation

Our results suggest that the PPnT also play a role in mediating innate behavior, more specifically in preventing behavioral adaptation to a stimulus. We are only beginning to understand the complex circuits and stimuli that induce innate behaviors. In the present study, we focus on a collicular-driven stopping behavior, which is akin to the startle-induced behavioral arrest observed when an animal is surprised by bright light or loud noise (Roseberry and Kreitzer, 2017). This rapid shift in attention and locomotion allows the animal to stop and survey the environment. We propose that the PPnT prevents habituation to stimuli inducing this behavior, ensuring that these innate responses to potential threats persist over repeated presentations of a stimulus. This has an evolutionary advantage, as ignoring repeated but relevant signs of a threat could be lethal. When we inhibit the PPnT, and more specifically the POL and PoT, we see an acceleration of this process of habituation. Without the PPnT, and in the absence of reinforcement, the innate reaction to the largely-neutral optogenetic stimulus is lost quickly. In normal functioning then, the PPnT does not allow a surprising stimulus to pass by unnoticed. The PPnT has been suggested to modify synaptic efficacy in the amygdala (McEchron et al., 1995) in the context of associative learning in auditory fear conditioning and fear extinction (Iwata et al., 1986; LeDoux et al., 1986; LeDoux et al., 1988; Romanski and LeDoux, 1992). We suggest that the PPnT could produce a similar modulatory effect in the amygdala in the collicular circuit, preventing habituation to unexpected stimuli based on its appraisal of information from the visual system. Examining our results in the context of previous research, we propose that the PPnT plays a vital role in conditioned and innate defensive behaviors involving multiple sensory systems.

4.4 Confirmation that wide-field neuron stimulation is sufficient to induce stopping

To confirm that targeted stimulation of wide-field neurons alone is sufficient to induce stopping, we injected AAV-ChR2 directly into the superior colliculus of NTSR1-Cre mice and compared their stopping behavior with that of Cre-negative NTSR x ChR2, and thus non-ChR2-expressing, controls. We found that optogenetic stimulation of ChR2-expressing wide-field neuron populations reliably induced stopping in NTSR1-Cre mice.

Our findings confirm that the stopping behavior we see in NTSR x ChR2 mice, which express ChR2 in all NTSR-positive neurons, is not solely due to non-specific stimulation of passing fibers or axon terminals of collicular inputs. In comparison to stopping episodes in NTSR x ChR2, the NTSR1-Cre mice tended to stop with less consistency, with episodes of shorter length. We propose that the number of excited cells determines the level of the response. Alternatively, it is possible that stimulation of collicular inputs in NTSR x ChR2 mice could augment the stopping effect. We also show that the behavioral attenuation resulting from chemogenetic PPnT inhibition is comparable in NTSR1-Cre and NTSR x ChR2 mice, confirming that outputs of wide-field neurons are implicated in the modified behavior.

The projection from the colliculus to the LP has garnered significant interest over recent years. Stimulation of CAMKII glutamatergic neurons from the intermediate layers of the medial superior colliculus induced innate, long-lasting freezing behavior as did stimulation of the colliculus-LP projection directly (Wei et al., 2015). A later study showed that selective activation of the colliculus-LP projection of PV+ neurons or activation of glutamatergic LP neurons invoked freezing, with the conclusion that glutamatergic PV+ neurons mediate this response (Shang et al., 2018). Here we show that stimulating wide-field neurons in the colliculus, which project to the LP alone, induces stopping episodes of shorter duration than freezing responses mediated by PV+ neurons. Similar episodes of temporary arrest have been induced by brief flashes of light and optogenetic stimulation of colliculus-projecting neurons in primary visual cortex (Liang et al., 2015), but it is not clear if and how wide-field neurons are a part of the same response. Recent work showing that wide-field neurons are necessary for rapid detection of prey (Hoy et al., 2019) supports the notion that these cells play a role in rapid detection of potential threats as well, inducing a winner-takes-all shift in attention leading to locomotive arrest to ensure proper environmental surveillance.

4.5 Technical considerations

Optogenetic and chemogenetic tools allow for targeted control of specific neuronal populations with high spatiotemporal specificity. There remain several caveats to keep in mind. In the present study, we use optogenetic stimulation as a proxy for visual stimulation. It is important to note that the precise role of wide-field neurons in natural visual behavior is still unknown. To approximate natural visual stimuli, we stimulated the superior colliculus at 20 Hz, the frequency observed to correlate to firing rates of natural visual responses in the colliculus (Wei et al., 2015). Additionally, it was recently confirmed in electrophysiological recordings that the PPnT is activated both by optogenetic stimulation of NTSR collicular neurons and visual stimuli (Sans-Dublanc et al., 2020). We use low laser power (0.2 mW) to avoid tissue heating from light delivery. Several implicit challenges in optogenetic studies remain, such as the invasiveness of fiber implantation and differential opsin expression between cells. To address these, we applied an angled implantation strategy and verified ChR2 expression histologically. Directly manipulating collicular circuits with optogenetics allows us to identify cause and effect relationships within these circuits and moves us closer to the ultimate goal of precisely explaining these circuits in a natural context.

The present study relies on unilateral inhibition of the PPnT. While immediate defensive responses are thought to be mediated mainly by ipsilateral pathways, the information is likely to spread to both hemispheres with consequent bilateral regulation. Therefore, we

posit that bilateral inhibition of the PPnT could have resulted in a stronger effect on behavior.

An important consideration for DREADD-mediated neural modulation with CNO is the potential for non-specific effects of CNO and its metabolite clozapine (Mahler and Aston-Jones, 2018; Gomez et al., 2017; Manvich et al., 2018). To control for potential off-target effects of CNO/clozapine, we administered CNO to a control group of non-DREADD-expressing animals. The control group was injected into the PPnT with an AAV carrying the gene for YFP as a reporter. Thus, DREADD and non-DREADD expressing animals underwent identical surgical treatment, behavioral testing, and CNO administration. Using this control confirms that the behavioral modifications we observed in DREADD animals were due to inhibition of the PPnT, and not due to non-specific binding of CNO on endogenous receptors. Reverse metabolism of CNO to clozapine reaches its peak at 2-3 hours after i.p. administration (Gomez et al., 2017), so we began our behavioral tests 30-40 minutes after CNO administration when clozapine levels are very low (7.4% clozapine to CNO ratio)(Manvich et al., 2018). We separated behavioral sessions by at least 48 hours to allow for clearance of the drug.

We recognize that using viral injections for gene delivery can introduce variability due to differences in diffusion, transfection, and expression from one injection to the next. This variability can be difficult to control for, which underscores the importance of histological analysis for accurate correlation with behavior. In our study, we aligned coronal sections of AAV-hM4D injections to the Allen Mouse Brain Atlas in order to have an accurate representation of the spread of the virus in each animal.

4.6 Future directions

Our identification of the PPnT as a part of the NTSR collicular downstream pathway presents exciting new directions of study. Looking forward, targeted AAV-hM4D injections of small quantities to specific nuclei of the PPnT could help elucidate the specific contributions of each nucleus, particularly the POL and PoT, to mediating stopping behavior. In this same thread, small, targeted injections of retrograde and anterograde tracers in each nucleus could clarify the picture of the complex circuitry involving this brain region. Single nuclei of the PPnT in rats are known to project differentially to cortical regions that transmit sensory information to the amygdala and hippocampus (Linke et al., 2000), so we could expect a similar pattern based on the correspondence of our tracing study with research in rats. It would also be interesting to inhibit the PPnT in a context of prey detection, as wide-field neurons are known to play an important part in this process. Another direction could involve a closer look at the auditory and somatosensory input to the PPnT. To understand collicular stopping behavior beyond the PPnT, future research could also involve an examination of the role of the VISpor and tail of the CPu in mediating stopping behavior, as these regions were also active in fUSi recordings during optogenetic stimulation of NTSR collicular neurons.

4.7 Conclusion

In conclusion, we show here that the PPnT modulates the rate of habituation to repeated stimulation of NTSR neurons in the superior colliculus, suppressing behavioral adaptation to potentially harmful stimuli. This study uncovers a novel place for the PPnT in this collicular circuit and in the study of visually-guided defensive behavior in general. As has

been shown here, efforts to understand circuits in mice and other small mammals could benefit greatly from using novel whole-brain imaging techniques to identify functional nodes and then directly manipulate them. We also give a first approximation here of the inputs to the PPnT in a mouse model. For the first time, we show that the PPnT is involved in innate behaviors and not only conditioned fear responses. Are there separate pathways for innate and conditioned fear circuits that project through the PPnT? Do they partially overlap, or are they completely independent? What are their specific functional contributions? Answering questions like these will ultimately bring us closer to understanding function and dysfunction in homologous circuits in humans.

5 References

Almeida, I., Soares, S.C., and Castelo-Branco, M. (2015). The Distinct Role of the Amygdala, Superior Colliculus and Pulvinar in Processing of Central and Peripheral Snakes. PLoS One*10*, e0129949.

Armbruster, B. N., Li, X., Pausch, M. H., Herlitze, S., & Roth, B. L. (2007). Evolving the lock to fit the key to create a family of G protein-coupled receptors potently activated by an inert ligand. Proceedings of the National Academy of Sciences of the United States of America, 104(12), 5163–5168. https://doi.org/10.1073/pnas.0700293104.

Arnault, P., and Roger, M. (1987). The connections of the peripeduncular area studied by retrograde and anterograde transport in the rat. J Comp Neurol*258*, 463–476.

Arnault, P., and Roger, M. (1990). Ventral temporal cortex in the rat: connections of secondary auditory areas Te2 and Te3. J Comp Neurol*302*, 110–123.

Asede, D., Bosch, D., Lüthi, A., Ferraguti, F., and Ehrlich, I. (2015). Sensory inputs to intercalated cells provide fear-learning modulated inhibition to the basolateral amygdala. Neuron*86*, 541–554.

Assareh, N., Sarrami, M., Carrive, P., and McNally, G.P. (2016). The organization of defensive behavior elicited by optogenetic excitation of rat lateral or ventrolateral periaqueductal gray. Behav Neurosci*130*, 406–414.

Bakker, R., Tiesinga, P., and Kötter, R. (2015). The Scalable Brain Atlas: Instant Web-Based Access to Public Brain Atlases and Related Content. Neuroinformatics*13*, 353–366.

Barth, D.S., and MacDonald, K.D. (1996). Thalamic modulation of high-frequency oscillating potentials in auditory cortex. Nature*383*, 78–81.

Basso, M.A., and May, P.J. (2017). Circuits for Action and Cognition: A View from the Superior Colliculus. Annu Rev Vis Sci*3*, 197–226.

Beltramo, R., and Scanziani, M. (2019). A collicular visual cortex: Neocortical space for an ancient midbrain visual structure. Science*363*, 64–69.

Benedek, G., Perény, J., Kovács, G., Fischer-Szátmári, L., and Katoh, Y.Y. (1997). Visual, somatosensory, auditory and nociceptive modality properties in the feline suprageniculate nucleus. Neuroscience*78*, 179–189.

Bennett, C., Gale, S.D., Garrett, M.E., Newton, M.L., Callaway, E.M., Murphy, G.J., and Olsen, S.R. (2019). Higher-Order Thalamic Circuits Channel Parallel Streams of Visual Information in Mice. Neuron*102*, 477–492.e5.

Bittencourt, A.S., Carobrez, A.P., Zamprogno, L.P., Tufik, S., and Schenberg, L.C. (2004). Organization of single components of defensive behaviors within distinct columns of periaqueductal gray matter of the rat: role of N-methyl-D-aspartic acid glutamate receptors. Neuroscience*125*, 71–89.

Bordi, F., and LeDoux, J.E. (1994). Response properties of single units in areas of rat auditory thalamus that project to the amygdala. I. Acoustic discharge patterns and frequency receptive fields. Exp Brain Res*98*, 261–274.

Bordi, F., and LeDoux, J.E. (1994). Response properties of single units in areas of rat auditory thalamus that project to the amygdala. II. Cells receiving convergent auditory and somatosensory inputs and cells antidromically activated by amygdala stimulation. Exp Brain Res*98*, 275–286.

Campeau, S., and Davis, M. (1995). Involvement of the central nucleus and basolateral complex of the amygdala in fear conditioning measured with fear-potentiated startle in rats trained concurrently with auditory and visual conditioned stimuli. J Neurosci*15*, 2301–2311.

Campeau, S., and Davis, M. (1995). Involvement of subcortical and cortical afferents to the lateral nucleus of the amygdala in fear conditioning measured with fear-potentiated startle in rats trained concurrently with auditory and visual conditioned stimuli. J Neurosci*15*, 2312–2327.

Carrive, P. (1993). The periaqueductal gray and defensive behavior: functional representation and neuronal organization. Behav Brain Res*58*, 27–47.

Chen, L., Wang, X., Ge, S., and Xiong, Q. (2019). Medial geniculate body and primary auditory cortex differentially contribute to striatal sound representations. Nat Commun*10*, 418.

Comoli, E., Das, N.F.P., Vautrelle, N., Leriche, M., Overton, P.G., and Redgrave, P. (2012). Segregated anatomical input to sub-regions of the rodent superior colliculus associated with approach and defense. Front Neuroanat*6*, 9.

Coolen, L.M., Veening, J.G., Petersen, D.W., and Shipley, M.T. (2003). Parvocellular subparafascicular thalamic nucleus in the rat: anatomical and functional compartmentalization. J Comp Neurol*463*, 117–131.

Cynader, M., and Berman, N. (1972). Receptive-field organization of monkey superior colliculus. J Neurophysiol*35*, 187–201.

De Franceschi G., Vivattanasarn, T., Saleem, A.B., and Solomon, S.G. (2016). Vision Guides Selection of Freeze or Flight Defense Strategies in Mice. Curr Biol*26*, 2150–2154.

Dean, P., Mitchell, I.J., and Redgrave, P. (1988). Responses resembling defensive behaviour produced by microinjection of glutamate into superior colliculus of rats. Neuroscience*24*, 501–510.

Dean, P., Redgrave, P., and Westby, G.W. (1989). Event or emergency? Two response systems in the mammalian superior colliculus. Trends Neurosci*12*, 137–147.

Deng, H., Xiao, X., and Wang, Z. (2016). Periaqueductal Gray Neuronal Activities Underlie Different Aspects of Defensive Behaviors. J Neurosci*36*, 7580–7588.

Doron, N.N., and Ledoux, J.E. (1999). Organization of projections to the lateral amygdala from auditory and visual areas of the thalamus in the rat. J Comp Neurol*412*, 383–409.

Dräger, U.C., and Hubel, D.H. (1975). Responses to visual stimulation and relationship between visual, auditory, and somatosensory inputs in mouse superior colliculus. J Neurophysiol*38*, 690–713.

Dräger, U.C., and Hubel, D.H. (1976). Topography of visual and somatosensory projections to mouse superior colliculus. J Neurophysiol*39*, 91–101.

DuBois, R.M., and Cohen, M.S. (2000). Spatiotopic organization in human superior colliculus observed with fMRI. Neuroimage*12*, 63–70.

Elsabbagh, M., Volein, A., Holmboe, K., Tucker, L., Csibra, G., Baron-Cohen, S., Bolton, P., Charman, T., Baird, G., and Johnson, M.H. (2009). Visual orienting in the early broader autism phenotype: disengagement and facilitation. J Child Psychol Psychiatry*50*, 637–642.

Evans, D.A., Stempel, A.V., Vale, R., Ruehle, S., Lefler, Y., and Branco, T. (2018). A synaptic threshold mechanism for computing escape decisions. Nature*558*, 590–594.

Franklin, G., K. & Paxinos (2019). Paxinos and Franklin's the Mouse Brain in Stereotaxic Coordinates, Compact(Academic Press).

Gale, S.D., and Murphy, G.J. (2014). Distinct representation and distribution of visual information by specific cell types in mouse superficial superior colliculus. J Neurosci*34*, 13458–13471.

Gale, S.D., and Murphy, G.J. (2018). Distinct cell types in the superficial superior colliculus project to the dorsal lateral geniculate and lateral posterior thalamic nuclei. J Neurophysiol*120*, 1286–1292.

Gerfen, C.R., Paletzki, R., and Heintz, N. (2013). GENSAT BAC cre-recombinase driver lines to study the functional organization of cerebral cortical and basal ganglia circuits. Neuron*80*, 1368–1383.

Gerren, R.A., and Weinberger, N.M. (1983). Long term potentiation in the magnocellular medial geniculate nucleus of the anesthetized cat. Brain Res*265*, 138–142.

Gomez, J.L., Bonaventura, J., Lesniak, W., Mathews, W.B., Sysa-Shah, P., Rodriguez, L.A., Ellis, R.J., Richie, C.T., Harvey, B.K., Dannals, R.F., et al. (2017). Chemogenetics revealed: DREADD occupancy and activation via converted clozapine. Science*357*, 503–507.

Goutaudier, R., Coizet, V., Carcenac, C., and Carnicella, S. (2019). DREADDs: The Power of the Lock, the Weakness of the Key. Favoring the Pursuit of Specific Conditions Rather than Specific Ligands. ENeuro*6*.

Guo, L., Walker, W.I., Ponvert, N.D., Penix, P.L., and Jaramillo, S. (2018). Stable representation of sounds in the posterior striatum during flexible auditory decisions. Nat Commun*9*, 1534.

Hicks, T.P., Stark, C.A., and Fletcher, W.A. (1986). Origins of afferents to visual suprageniculate nucleus of the cat. J Comp Neurol*246*, 544–554.

Hicks, T.P., Watanabe, S., Miyake, A., and Shoumura, K. (1984). Organization and properties of visually responsive neurones in the suprageniculate nucleus of the cat. Exp Brain Res*55*, 359–367.

Hoy, J.L., Bishop, H.I., and Niell, C.M. (2019). Defined Cell Types in Superior Colliculus Make Distinct Contributions to Prey Capture Behavior in the Mouse. Curr Biol*29*, 4130–4138.e5.

Hunnicutt, B.J., Jongbloets, B.C., Birdsong, W.T., Gertz, K.J., Zhong, H., and Mao, T. (2016). A comprehensive excitatory input map of the striatum reveals novel functional organization. Elife*5*.

Ito, S., and Feldheim, D.A. (2018). The Mouse Superior Colliculus: An Emerging Model for Studying Circuit Formation and Function. Front Neural Circuits*12*, 10.

Iwata, J., LeDoux, J.E., Meeley, M.P., Arneric, S., and Reis, D.J. (1986). Intrinsic neurons in the amygdaloid field projected to by the medial geniculate body mediate emotional responses conditioned to acoustic stimuli. Brain Res*383*, 195–214.

Jhang, J., Lee, H., Kang, M.S., Lee, H.S., Park, H., and Han, J.H. (2018). Anterior cingulate cortex and its input to the basolateral amygdala control innate fear response. Nat Commun*9*, 2744.

Jones, E.G. (1998). A new view of specific and nonspecific thalamocortical connections. Adv Neurol*77*, 49–71; discussion 72–73.

Jones, E.G. (1998). Viewpoint: the core and matrix of thalamic organization. Neuroscience*85*, 331–345.

Kamishina, H., Yurcisin, G.H., Corwin, J.V., and Reep, R.L. (2008). Striatal projections from the rat lateral posterior thalamic nucleus. Brain Res*1204*, 24–39.

Katyal, S., Zughni, S., Greene, C., and Ress, D. (2010). Topography of covert visual attention in human superior colliculus. J Neurophysiol*104*, 3074–3083.

Keifer, O.P.J., Gutman, D.A., Hecht, E.E., Keilholz, S.D., and Ressler, K.J. (2015). A comparative analysis of mouse and human medial geniculate nucleus connectivity: a DTI and anterograde tracing study. Neuroimage*105*, 53–66.

Keifer, O.P.J, Hurt, R.C., Ressler, K.J., Marvar, P.J. (2015). The Physiology of Fear: Reconceptualizing the Role of the Central Amygdala in Fear Learning. *Physiology (Bethesda)* 30, 389-401.

Kincheski, G.C., Mota-Ortiz, S.R., Pavesi, E., Canteras, N.S., and Carobrez, A.P. (2012). The dorsolateral periaqueductal gray and its role in mediating fear learning to life threatening events. PLoS One*7*, e50361.

Krauzlis, R.J., Bollimunta, A., Arcizet, F., and Wang, L. (2014). Attention as an effect not a cause. Trends Cogn Sci*18*, 457–464.

Krupa, M., Maire-Lepoivre, E., and Imbert, M. (1984). Visual properties of neurons in the suprageniculate nucleus of the cat. Neurosci Lett*51*, 13–18.

Kunwar, P.S., Zelikowsky, M., Remedios, R., Cai, H., Yilmaz, M., Meister, M., and Anderson, D.J. (2015). Ventromedial hypothalamic neurons control a defensive emotion state. Elife*4*.

LeDoux, J.E. (2000). Emotion circuits in the brain. Annu Rev Neurosci*23*, 155–184.

LeDoux, J.E., Farb, C.R., and Romanski, L.M. (1991). Overlapping projections to the amygdala and striatum from auditory processing areas of the thalamus and cortex. Neurosci Lett*134*, 139–144.

LeDoux, J.E., Iwata, J., Cicchetti, P., and Reis, D.J. (1988). Different projections of the central amygdaloid nucleus mediate autonomic and behavioral correlates of conditioned fear. J Neurosci*8*, 2517–2529.

LeDoux, J.E., Ruggiero, D.A., and Reis, D.J. (1985). Projections to the subcortical forebrain from anatomically defined regions of the medial geniculate body in the rat. J Comp Neurol*242*, 182–213.

LeDoux, J.E., Sakaguchi, A., Iwata, J., and Reis, D.J. (1985). Auditory emotional memories: establishment by projections from the medial geniculate nucleus to the posterior neostriatum and/or dorsal amygdala. Ann N Y Acad Sci*444*, 463–464.

LeDoux, J.E., Sakaguchi, A., Iwata, J., and Reis, D.J. (1986). Interruption of projections from the medial geniculate body to an archi-neostriatal field disrupts the classical conditioning of emotional responses to acoustic stimuli. Neuroscience*17*, 615–627.

LeDoux, J.E., Sakaguchi, A., and Reis, D.J. (1984). Subcortical efferent projections of the medial geniculate nucleus mediate emotional responses conditioned to acoustic stimuli. J Neurosci*4*, 683–698.

Ledoux, J.E., Ruggiero, D.A., Forest, R., Stornetta, R., and Reis, D.J. (1987). Topographic organization of convergent projections to the thalamus from the inferior colliculus and spinal cord in the rat. J Comp Neurol*264*, 123–146.

Ledoux, J.E., and Muller, J. (1997). Emotional memory and psychopathology. Philos Trans R Soc Lond B Biol Sci*352*, 1719–1726.

Liang, F., Xiong, X.R., Zingg, B., Ji, X.Y., Zhang, L.I., and Tao, H.W. (2015). Sensory Cortical Control of a Visually Induced Arrest Behavior via Corticotectal Projections. Neuron*86*, 755–767.

Linke, R. (1999). Differential projection patterns of superior and inferior collicular neurons onto posterior paralaminar nuclei of the thalamus surrounding the medial geniculate body in the rat. Eur J Neurosci*11*, 187–203.

Linke, R., Braune, G., and Schwegler, H. (2000). Differential projection of the posterior paralaminar thalamic nuclei to the amygdaloid complex in the rat. Exp Brain Res*134*, 520–532.

Linke, R., De, L.A.D., Schwegler, H., and Pape, H.C. (1999). Direct synaptic connections of axons from superior colliculus with identified thalamo-amygdaloid projection neurons in the rat: possible substrates of a subcortical visual pathway to the amygdala. J Comp Neurol*403*, 158–170.

Linke, R., and Schwegler, H. (2000). Convergent and complementary projections of the caudal paralaminar thalamic nuclei to rat temporal and insular cortex. Cereb Cortex*10*, 753–771.

Macé, É., Montaldo, G., Trenholm, S., Cowan, C., Brignall, A., Urban, A., and Roska, B. (2018). Whole-Brain Functional Ultrasound Imaging Reveals Brain Modules for Visuomotor Integration. Neuron*100*, 1241–1251.e7.

Madisen, L., Zwingman, T.A., Sunkin, S.M., Oh, S.W., Zariwala, H.A., Gu, H., Ng, L.L., Palmiter, R.D., Hawrylycz, M.J., Jones, A.R., et al. (2010). A robust and high-throughput Cre reporting and characterization system for the whole mouse brain. Nat Neurosci*13*, 133–140.

Mahler, S.V., and Aston-Jones, G. (2018). CNO Evil? Considerations for the Use of DREADDs in Behavioral Neuroscience. Neuropsychopharmacology*43*, 934–936.

Manvich, D.F., Webster, K.A., Foster, S.L., Farrell, M.S., Ritchie, J.C., Porter, J.H., and Weinshenker, D. (2018). The DREADD agonist clozapine N-oxide (CNO) is reverse-metabolized to clozapine and produces clozapine-like interoceptive stimulus effects in rats and mice. Sci Rep*8*, 3840.

Maren, S. (2011). Seeking a spotless mind: extinction, deconsolidation, and erasure of fear memory. Neuron*70*, 830–845.

Maren, S. (2001). Neurobiology of Pavlovian fear conditioning. Annu Rev Neurosci*24*, 897–931.

Mathis, A., Mamidanna, P., Cury, K.M., Abe, T., Murthy, V.N., Mathis, M.W., and Bethge, M. (2018). DeepLabCut: markerless pose estimation of user-defined body parts with deep learning.Nature Neuroscience*21*, 1281–1289.

Mathis, M.W., and Mathis, A. (2020). Deep learning tools for the measurement of animal behavior in neuroscience. Curr Opin Neurobiol*60*, 1–11.

Mattis, J., Tye, K.M., Ferenczi, E.A., Ramakrishnan, C., O'Shea, D.J., Prakash, R., Gunaydin, L.A., Hyun, M., Fenno, L.E., Gradinaru, V., et al. (2011). Principles for applying optogenetic tools derived from direct comparative analysis of microbial opsins. Nat Methods*9*, 159–172.

May, P.J. (2006). The mammalian superior colliculus: laminar structure and connections. Prog Brain Res*151*, 321–378.

McEchron, M.D., Green, E.J., Winters, R.W., Nolen, T.G., Schneiderman, N., and McCabe, P.M. (1996). Changes of synaptic efficacy in the medial geniculate nucleus as a result of auditory classical conditioning. J Neurosci*16*, 1273–1283.

McEchron, M.D., McCabe, P.M., Green, E.J., Llabre, M.M., and Schneiderman, N. (1995). Simultaneous single unit recording in the medial nucleus of the medial geniculate nucleus and amygdaloid central nucleus throughout habituation, acquisition, and extinction of the rabbit's classically conditioned heart rate. Brain Res*682*, 157–166.

McHaffie, J.G., Jiang, H., May, P.J., Coizet, V., Overton, P.G., Stein, B.E., and Redgrave, P. (2006). A direct projection from superior colliculus to substantia nigra pars compacta in the cat. Neuroscience*138*, 221–234.

Meyer, C., Padmala, S., and Pessoa, L. (2019). Dynamic Threat Processing. J Cogn Neurosci*31*, 522–542.

Mitchell, I.J., Dean, P., and Redgrave, P. (1988). The projection from superior colliculus to cuneiform area in the rat. II. Defence-like responses to stimulation with glutamate in cuneiform nucleus and surrounding structures. Exp Brain Res*72*, 626–639.

Mongeau, R., Miller, G.A., Chiang, E., and Anderson, D.J. (2003). Neural correlates of competing fear behaviors evoked by an innately aversive stimulus. J Neurosci*23*, 3855–3868.

Moriizumi, T., and Hattori, T. (1992). Ultrastructural morphology of projections from the medial geniculate nucleus and its adjacent region to the basal ganglia. Brain Res Bull*29*, 193–198.

Nakamura, H., Hioki, H., Furuta, T., and Kaneko, T. (2015). Different cortical projections from three subdivisions of the rat lateral posterior thalamic nucleus: a single-neuron tracing study with viral vectors. Eur J Neurosci*41*, 1294–1310.

Namura, S., Takada, M., Kikuchi, H., and Mizuno, N. (1997). Collateral projections of single neurons in the posterior thalamic region to both the temporal cortex and the amygdala: a fluorescent retrograde double-labeling study in the rat. J Comp Neurol*384*, 59–70.

Nath, T., Mathis, A., Chen, A.C., Patel, A., Bethge, M., and Mathis, M.W. (2019). Using DeepLabCut for 3D markerless pose estimation across species and behaviors.Nature Protocols*14*, 2152–2176.

Olivé, I., Densmore, M., Harricharan, S., Théberge, J., McKinnon, M.C., and Lanius, R. (2018). Superior colliculus resting state networks in post-traumatic stress disorder and its dissociative subtype. Hum Brain Mapp*39*, 563–574.

Peschanski, M. (1984). Trigeminal afferents to the diencephalon in the rat. Neuroscience*12*, 465–487.

Ponvert, N.D., and Jaramillo, S. (2019). Auditory Thalamostriatal and Corticostriatal Pathways Convey Complementary Information about Sound Features. J Neurosci*39*, 271–280.

Redgrave, P., Coizet, V., Comoli, E., McHaffie, J.G., Leriche, M., Vautrelle, N., Hayes, L.M., and Overton, P. (2010). Interactions between the Midbrain Superior Colliculus and the Basal Ganglia. Front Neuroanat*4*.

Romanski, L.M., and LeDoux, J.E. (1992). Equipotentiality of thalamo-amygdala and thalamo-cortico-amygdala circuits in auditory fear conditioning. J Neurosci*12*, 4501–4509.

Roseberry, T., and Kreitzer, A. (2017). Neural circuitry for behavioural arrest. Philos Trans R Soc Lond B Biol Sci*372*.

Ryugo, D.K., and Weinberger, N.M. (1978). Differential plasticity of morphologically distinct neuron populations in the medical geniculate body of the cat during classical conditioning. Behav Biol*22*, 275–301.

Sahibzada, N., Dean, P., and Redgrave, P. (1986). Movements resembling orientation or avoidance elicited by electrical stimulation of the superior colliculus in rats. J Neurosci*6*, 723–733.

Sans-Dublanc, A., Chrzanowska, A., Reinhard, K., Lemmon, D., Montaldo, G., Urban, A., and Farrow, K. (2020). Brain-wide mapping of neural activity mediating collicular-dependent behaviors.BioRxiv.

Schneider, K.A., and Kastner, S. (2005). Visual responses of the human superior colliculus: a high-resolution functional magnetic resonance imaging study. J Neurophysiol*94*, 2491–2503.

Senatorov, V.V., and Hu, B. (2002). Extracortical descending projections to the rat inferior colliculus. Neuroscience*115*, 243–250.

Sewards, T.V., and Sewards, M.A. (2002). Innate visual object recognition in vertebrates: some proposed pathways and mechanisms. Comp Biochem Physiol A Mol Integr Physiol*132*, 861–891.

Shamash, P., Carandini, M., Harris, K.D., and Steinmetz, N.A. (2018). A tool for analyzing electrode tracks from slice histology.

Shammah-Lagnado, S.J., Alheid, G.F., and Heimer, L. (1996). Efferent connections of the caudal part of the globus pallidus in the rat. J Comp Neurol*376*, 489–507.

Shang, C., Chen, Z., Liu, A., Li, Y., Zhang, J., Qu, B., Yan, F., Zhang, Y., Liu, W., Liu, Z., et al. (2018). Divergent midbrain circuits orchestrate escape and freezing responses to looming stimuli in mice. Nat Commun*9*, 1232.

Shang, C., Liu, Z., Chen, Z., Shi, Y., Wang, Q., Liu, S., Li, D., and Cao, P. (2015). BRAIN CIRCUITS. A parvalbumin-positive excitatory visual pathway to trigger fear responses in mice. Science*348*, 1472–1477.

Silva, B.A., Gross, C.T., and Gräff, J. (2016). The neural circuits of innate fear: detection, integration, action, and memorization. Learn Mem*23*, 544–555.

Soares, S.C., Kessel, D., Hernández-Lorca, M., García-Rubio, M.J., Rodrigues, P., Gomes, N., and Carretié, L. (2017). Exogenous attention to fear: Differential behavioral and neural responses to snakes and spiders. Neuropsychologia*99*, 139–147.

Soares, S.C., Maior, R.S., Isbell, L.A., Tomaz, C., and Nishijo, H. (2017a). Fast Detector/First Responder: Interactions between the Superior Colliculus-Pulvinar Pathway and Stimuli Relevant to Primates. Front Neurosci*11*, 67.

Sparks, D.L., Lee, C., and Rohrer, W.H. (1990). Population coding of the direction, amplitude, and velocity of saccadic eye movements by neurons in the superior colliculus. Cold Spring Harb Symp Quant Biol*55*, 805–811.

Sukov, W., and Barth, D.S. (2001). Cellular mechanisms of thalamically evoked gamma oscillations in auditory cortex. J Neurophysiol*85*, 1235–1245.

Takada, M., Itoh, K., Yasui, Y., Sugimoto, T., and Mizuno, N. (1985). Topographical projections from the posterior thalamic regions to the striatum in the cat, with reference to possible tecto-thalamo-striatal connections. Exp Brain Res*60*, 385–396.

Tanaka, K., Otani, K., Tokunaga, A., and Sugita, S. (1985). The reciprocal connections of the suprageniculate nucleus and the superior colliculus in the rat. Neurosci Res*3*, 79–85.

Terpou, B.A., Densmore, M., Théberge, J., Thome, J., Frewen, P., McKinnon, M.C., and Lanius, R.A. (2019). The Threatful Self: Midbrain Functional Connectivity to Cortical Midline and Parietal Regions During Subliminal Trauma-Related Processing in PTSD. Chronic Stress (Thousand Oaks)*3*, 2470547019871369.

Thakkar, K.N., Schall, J.D., Heckers, S., and Park, S. (2015). Disrupted Saccadic Corollary Discharge in Schizophrenia. J Neurosci*35*, 9935–9945.

Thakkar, K.N., and Rolfs, M. (2019). Disrupted Corollary Discharge in Schizophrenia: Evidence From the Oculomotor System. Biol Psychiatry Cogn Neurosci Neuroimaging*4*, 773–781.

Tohmi, M., Meguro, R., Tsukano, H., Hishida, R., and Shibuki, K. (2014). The extrageniculate visual pathway generates distinct response properties in the higher visual areas of mice. Curr Biol*24*, 587–597.

Urban, A., Mace, E., Brunner, C., Heidmann, M., Rossier, J., and Montaldo, G. (2014). Chronic assessment of cerebral hemodynamics during rat forepaw electrical stimulation using functional ultrasound imaging. Neuroimage*101*, 138–149.

Vagnoni, E., Lourenco, S.F., and Longo, M.R. (2015). Threat modulates neural responses to looming visual stimuli. Eur J Neurosci*42*, 2190–2202.

Vagnoni, E., Lourenco, S.F., and Longo, M.R. (2012). Threat modulates perception of looming visual stimuli. Curr Biol*22*, R826–7.

Vianna, D.M., and Brandão, M.L. (2003). Anatomical connections of the periaqueductal gray: specific neural substrates for different kinds of fear. Braz J Med Biol Res*36*, 557–566.

Villalobos, C.A., Wu, Q., Lee, P.H., May, P.J., and Basso, M.A. (2018). Parvalbumin and GABA Microcircuits in the Mouse Superior Colliculus. Front Neural Circuits*12*, 35.

Vlamings, P.H., Jonkman, L.M., van, D.E., van, der G.R.J., and Kemner, C. (2010). Basic abnormalities in visual processing affect face processing at an early age in autism spectrum disorder. Biol Psychiatry*68*, 1107–1113.

Wallace, D.J., Greenberg, D.S., Sawinski, J., Rulla, S., Notaro, G., and Kerr, J.N. (2013). Rats maintain an overhead binocular field at the expense of constant fusion. Nature*498*, 65–69.

Wang, X., Chou, X., Peng, B., Shen, L., Huang, J.J., Zhang, L.I., and Tao, H.W. (2019). A cross-modality enhancement of defensive flight via parvalbumin neurons in zona incerta. Elife*8*.

Wang, Y.C., Bianciardi, M., Chanes, L., and Satpute, A.B. (2020). Ultra High Field fMRI of Human Superior Colliculi Activity during Affective Visual Processing. Sci Rep*10*, 1331.

Watson, C. (2012). Visual System.In The Mouse Nervous System,(Elsevier),pp.646–652.

Wei, P., Liu, N., Zhang, Z., Liu, X., Tang, Y., He, X., Wu, B., Zhou, Z., Liu, Y., Li, J., et al. (2015). Processing of visually evoked innate fear by a non-canonical thalamic pathway. Nat Commun*6*, 6756.

Wei, P., Liu, N., Zhang, Z., Liu, X., Tang, Y., He, X., Wu, B., Zhou, Z., Liu, Y., Li, J., et al. (2015). Corrigendum: Processing of visually evoked innate fear by a non-canonical thalamic pathway. Nat Commun*6*, 8228.

Wepsic, J.G. (1966). Multimodal sensory activation of cells in the magnocellular medial geniculate nucleus. Exp Neurol*15*, 299–318.

Wilhelmi, E., Linke, R., de, L.A.D., and Pape, H.C. (2001). Axonal connections of thalamic posterior paralaminar nuclei with amygdaloid projection neurons to the cholinergic basal forebrain in the rat. Neurosci Lett*315*, 121–124.

Winer, J.A., Chernock, M.L., Larue, D.T., and Cheung, S.W. (2002). Descending projections to the inferior colliculus from the posterior thalamus and the auditory cortex in rat, cat, and monkey. Hear Res*168*, 181–195.

Winer, J.A., and Larue, D.T. (1988). Anatomy of glutamic acid decarboxylase immunoreactive neurons and axons in the rat medial geniculate body. J Comp Neurol*278*, 47–68.

Winer, J.A., and Morest, D.K. (1983). The medial division of the medial geniculate body of the cat: implications for thalamic organization. J Neurosci*3*, 2629–2651.

Xiong, X.R., Liang, F., Zingg, B., Ji, X.Y., Ibrahim, L.A., Tao, H.W., and Zhang, L.I. (2015). Auditory cortex controls sound-driven innate defense behaviour through corticofugal projections to inferior colliculus. Nat Commun*6*, 7224.

Yasui, Y., Kayahara, T., Nakano, K., and Mizuno, N. (1990). The subparafascicular thalamic nucleus of the rat receives projection fibers from the inferior colliculus and auditory cortex. Brain Res*537*, 323–327.

Yilmaz, M., and Meister, M. (2013). Rapid innate defensive responses of mice to looming visual stimuli. Curr Biol*23*, 2011–2015.

Zhou, N., Masterson, S.P., Damron, J.K., Guido, W., and Bickford, M.E. (2018). The Mouse Pulvinar Nucleus Links the Lateral Extrastriate Cortex, Striatum, and Amygdala. J Neurosci*38*, 347–362.

Appendix A |

Table S1. Video links and descriptions

Link	Related Figure	Description
Video S1	Figure 6	**DeepLabCut labeled markers.** Video clip showing labeled markers (nose, ears, tail base, and tail end) assigned by DeepLabCut software. Tail base marker was used for speed extraction.
Video S2	Figure 7	**Session 1: Mice display consistent stopping behavior during early and late trials.** Video compilation of Session 1 open-field testing for a mouse expressing hM4D in the PPnT (n=1) and a YFP-expressing control (n=1). Saline was injected in this session. One early and one late trial is shown for each mouse. Early trials were taken from among first three stimulation trials, and late trials were taken from final three stimulation trials. The text "STIM" appears in the bottom right corner to indicate the 1 second optogenetic stimulation.
Video S3	Figure 7	**Session 2: Inhibition of the PPnT facilitates habituation to stimulation of Ntsr+ neurons.** Video compilation of Session 2 open-field testing for a mouse expressing hM4D in the PPnT (n=1) and a YFP-expressing control (n=1). CNO was injected in this session to inhibit the PPnT in hM4D-expressing mice. One early and one late trial is shown for each mouse. Early trials were taken from among first three stimulation trials, and late trials were taken from final three stimulation trials. The text "STIM" appears in the bottom right corner to indicate the 1 second optogenetic stimulation.
Video S4	Figure 9	**Stimulation of wide-field neurons is sufficient to elicit stopping behavior.** Video compilation of open-field testing for an Ntsr1-Cre mouse injected with AAV-ChR2 in the superior colliculus for targeted stimulation of wide-field neurons (n=1) and one Cre negative control (n=1). The text "STIM" appears in the bottom right corner to indicate the 1 second optogenetic stimulation.
Video S5	Figure 10	**Ntsr1-Cre mice display behavioral trends comparable to Ntsr x ChR2 mice upon PPnT inhibition.** Video compilation from open field testing for an Ntsr1-Cre mouse (n=1) expressing ChR2 in wide-field neurons and hM4D in the PPnT. In Session 1, mouse was injected with saline, and in Session 2 mouse was injected with CNO to inhibit the PPnT. The text "STIM" appears in bottom right corner during the 1 second optogenetic stimulation.

Appendix B | Supplementary Figures

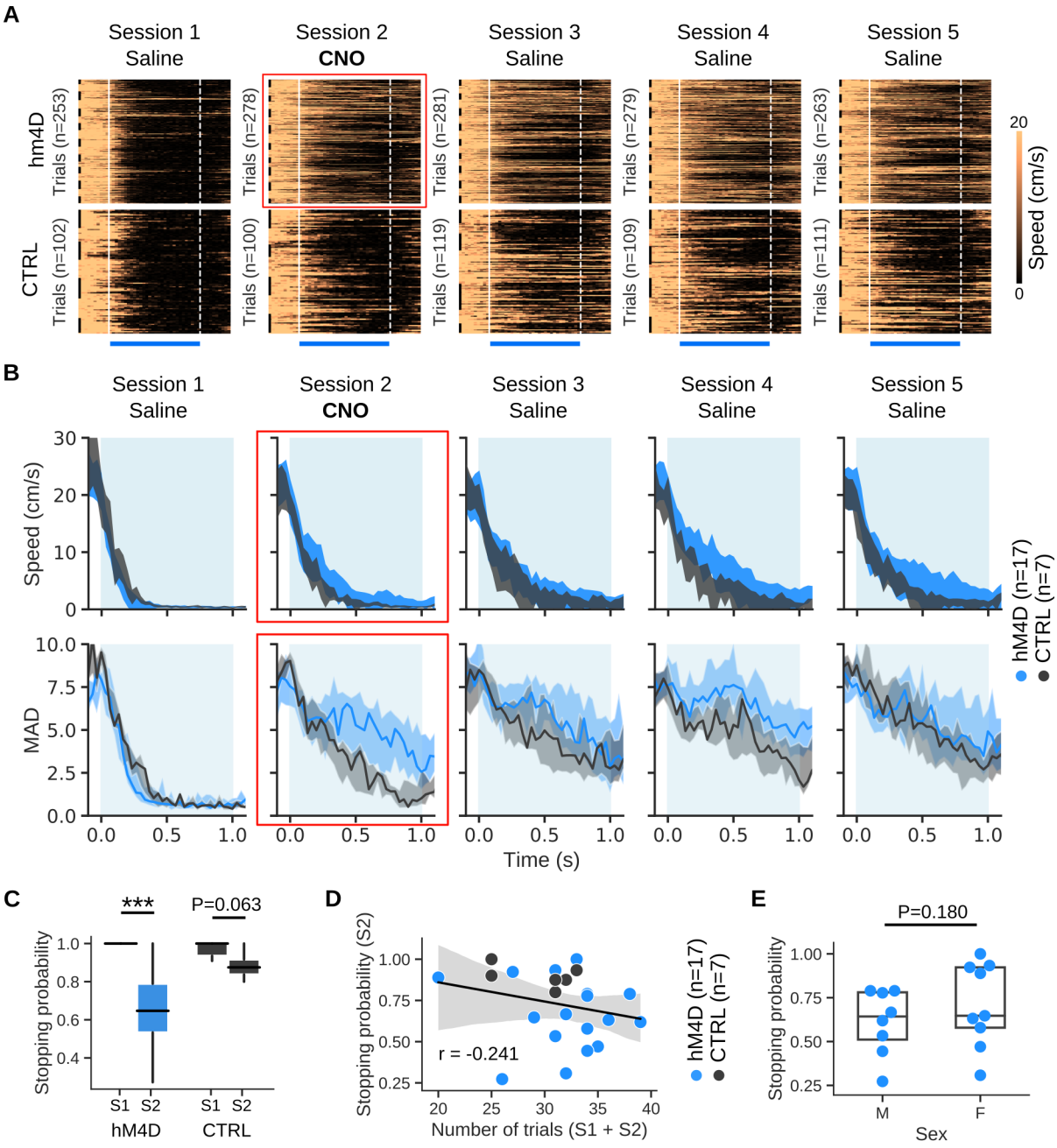

FIGURE S1 | PPnT inhibition facilitates habituation to stimulation of NTSR collicular neurons. A. Heatmaps showing speed over time for NTSR x Chr2 AAV-hM4D mice (top row, n=17) and AAV-YFP controls (bottom row, n=7) during the 1 s stimulation for all five sessions. Each row is a single trial, and trials belonging to a single animal are indicated by the vertical black lines on the left of the plot. Blue rectangle (bottom) indicates when laser was on, and vertical white lines show stimulus onset and offset. **B.** Top row, median speed over time of all hM4D (blue) and control (gray) mice for all 5 sessions, zoomed in on the 1 s stimulation. Bottom row, mean absolute deviation (MAD) in speeds across trials for hM4D (blue) and CTRL (gray) animals, zoomed in on the 1 s stimulation. **A-B.** Red box indicates plots where PPnT is inhibited in hM4D mice. **C.** Paired comparison of difference in stopping probability between Session 1 (saline) and Session 2 (CNO) for hM4D (blue, n=17; Wilcoxon signed-rank test; *P*=0.0004) and CTRL animals (gray, n=7; *P*=0.063). **D.** Correlation of stopping probability in Session 2 (when CNO was adminis-

tered) and the number of trials in Session 1 and 2 combined for hM4D (blue, n=17) and CTRL (gray, n=7) animals (Pearson correlation coefficient; r = -0.241). **E.** Comparison of stopping probability in Session 2 (CNO) for male (n=8) and female mice (n=9) in the hM4D group (Mann-Whitney U test; *P*=0.180). *** $P < 0.001$

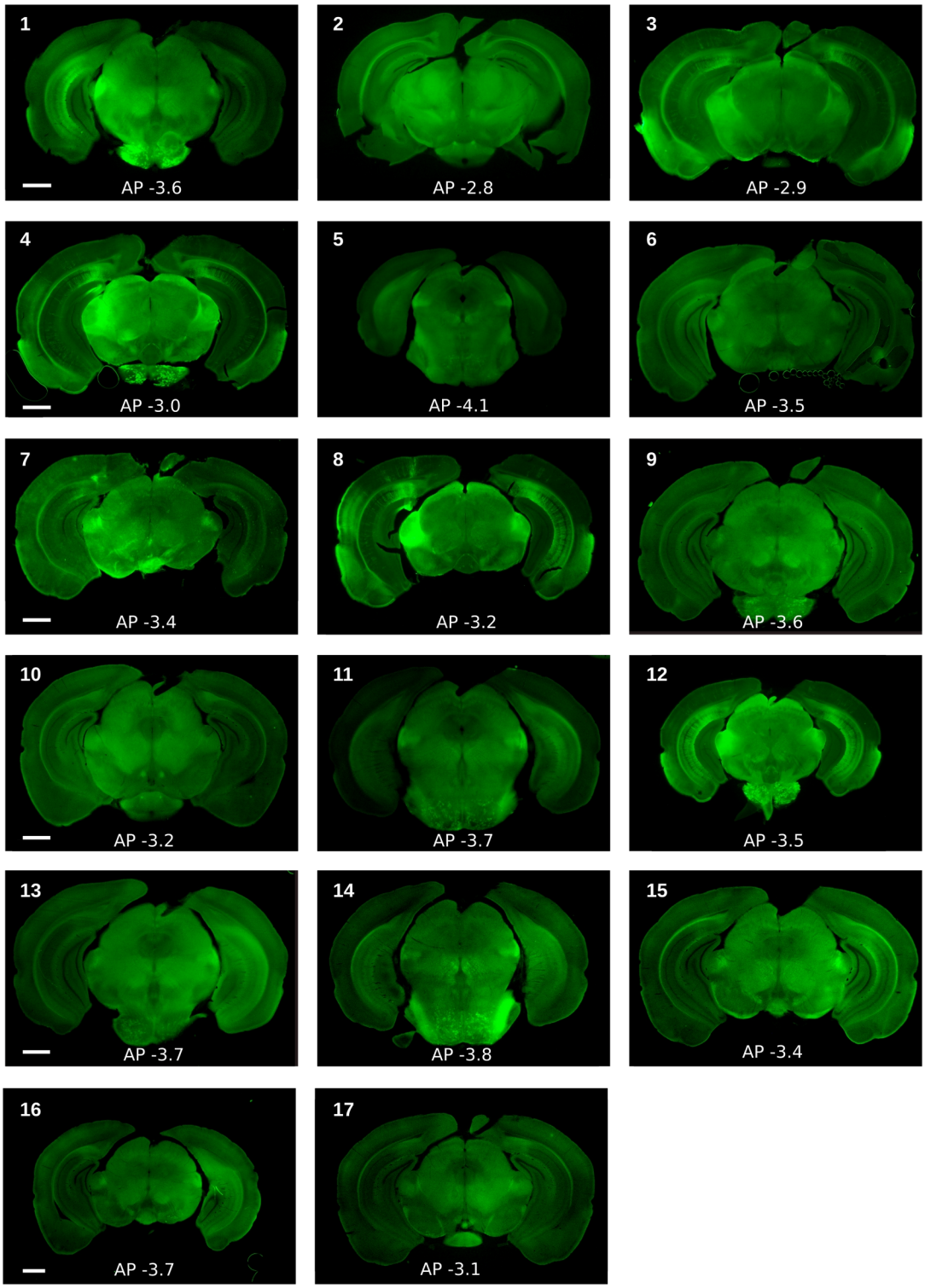

FIGURE S2 | Optic fiber placements of hM4D-expressing mice. Coronal sections of mice in hM4D group (n=17) showing AP position of the fiber tip for each animal. Animal numbers (top left corner of each image) correspond to the numbered images in Fig S3. Animals are numbered based on stopping probability in Session 2, in which CNO was administered, with 1 being the animal with the lowest stopping probability (0.27) and 17 being the animal with the highest (1.0). Scale bar, 1 mm.

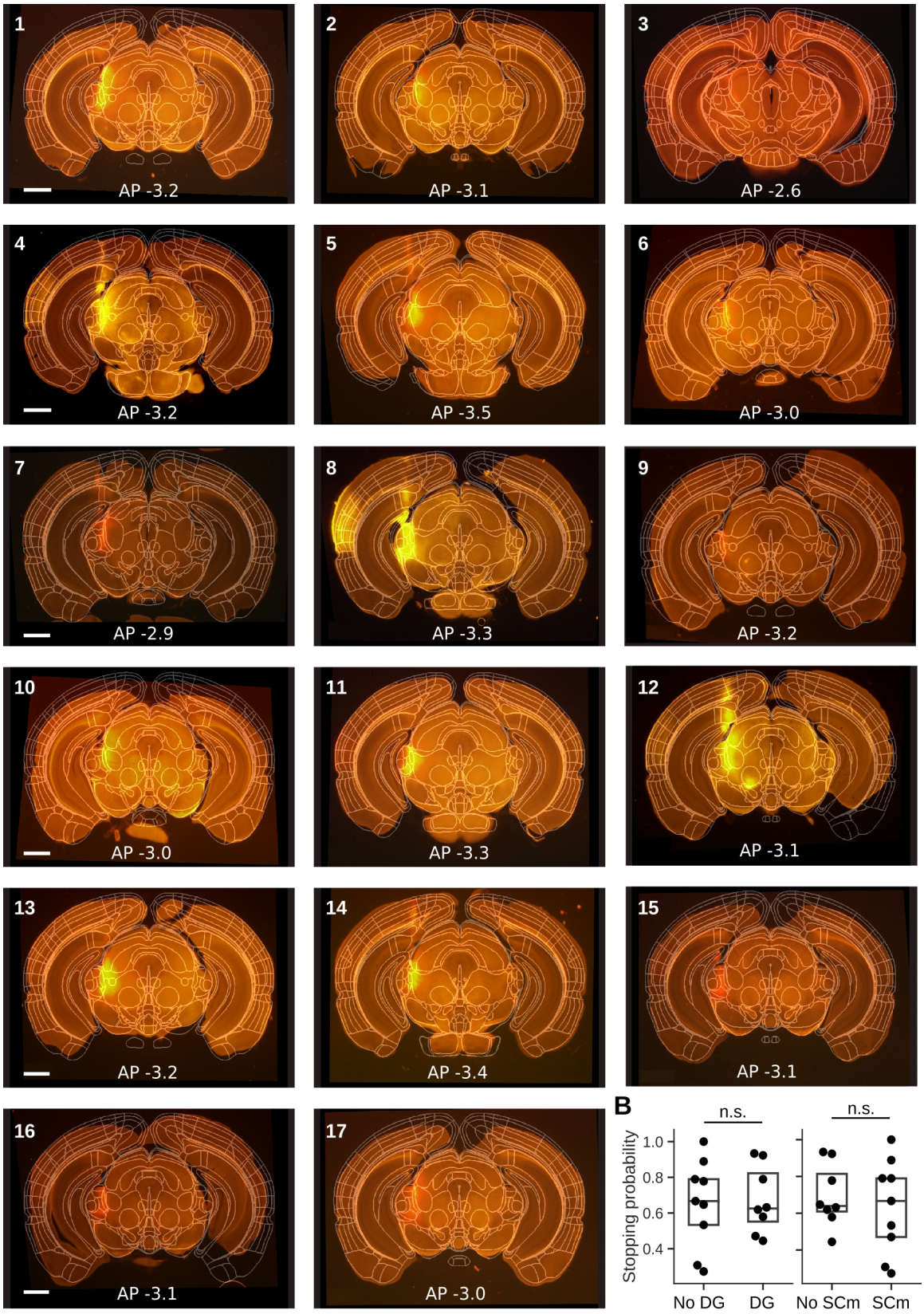

FIGURE S3 | Center of hM4D expression. A. Coronal sections aligned to the Allen Reference Atlas showing the center of AAV-hM4D expression for each animal on the AP plane (n=17). Animal numbers (top left corner of each image) correspond to the numbered fiber images in Figure S2. Animals are numbered based on stopping probability in Session 2, in which CNO was administered, with 1 being the animal with the lowest stopping probability (0.27) and 17 being the animal

with the highest (1.0). Scale bar, 1 mm. **B.** Stopping probability of AAV-hM4D mice with and without expression in the dentate gyrus (DG, left) and superior colliculus, motor related areas (SCm, right). Box plots indicate median and IQR. Significance was tested using Mann-Whitney U-test (alpha = 0.05).

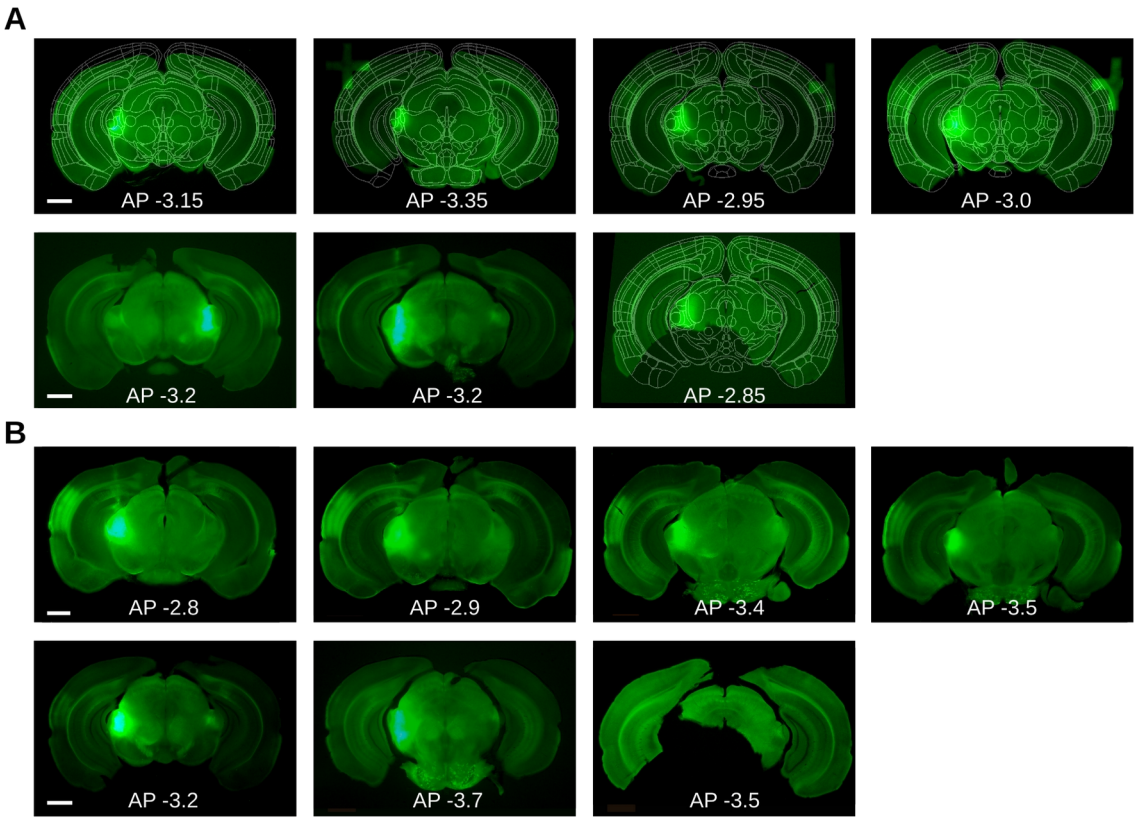

FIGURE S4 | Histological validation for AAV-YFP controls. A. Coronal sections, aligned to the Allen Reference Atlas, showing center of AAV-YFP expression in control mice, one image per mouse (n=7). Scale bar, 1 mm. **B.** Coronal sections showing AP position of fiber tip, one image per mouse (n=7). Scale bar, 1 mm. Order of animals in panel A corresponds to order in B.

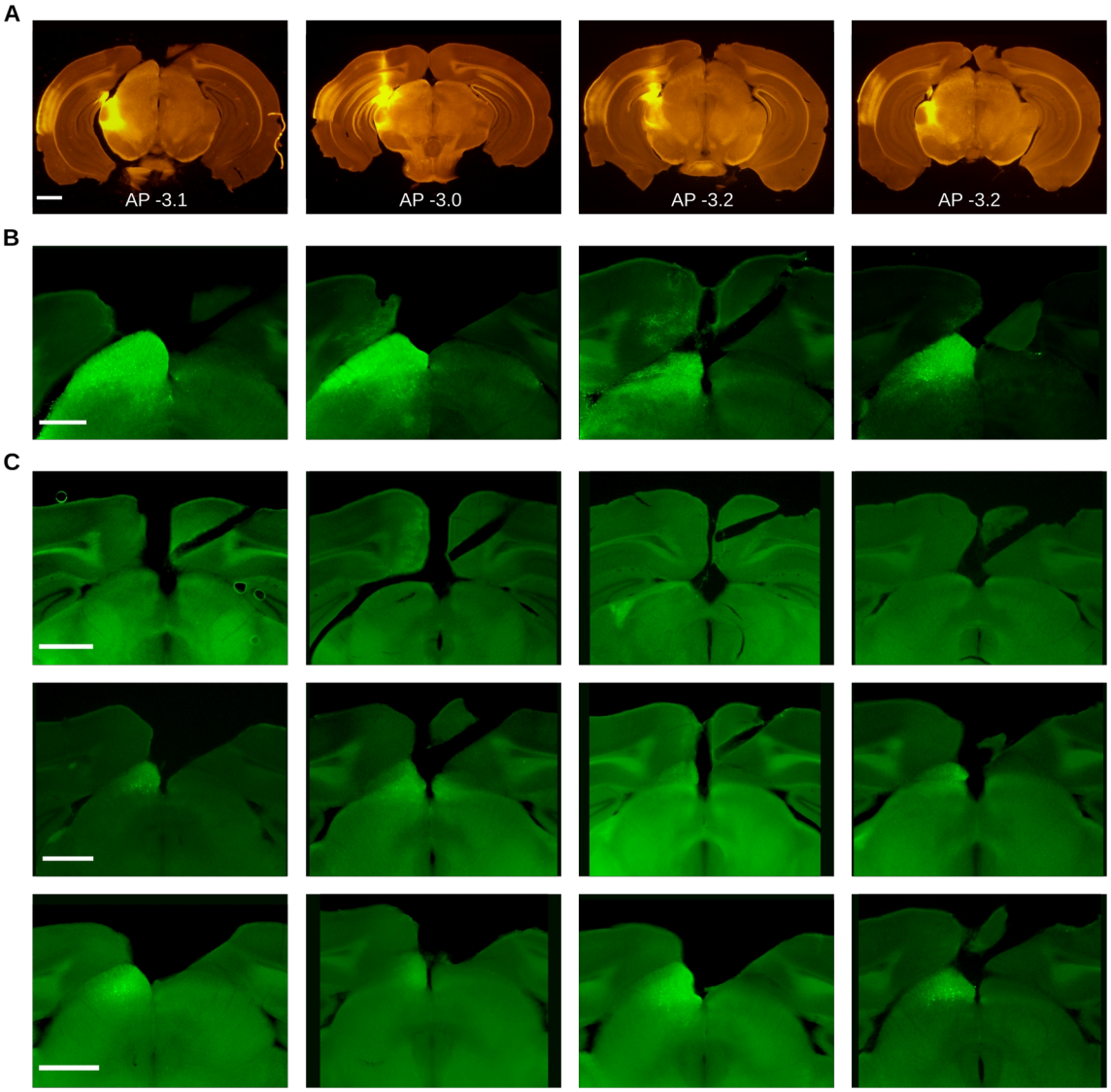

FIGURE S5 | Histological validation for NTSR1-Cre mice. A. Coronal sections showing AAV-hM4D expression in NTSR1-Cre mice, one image per mouse (n=4). **B.** Coronal sections showing ChR2 expression aligned with fiber tip in NTSR1-Cre responsive mice, one image per mouse (n=4). Order of animals in panel A corresponds to B. **C.** Coronal sections showing little to no ChR2 aligned with fiber tip in NTSR1-Cre non-responsive mice (n=12). Scale bar, 1 mm.

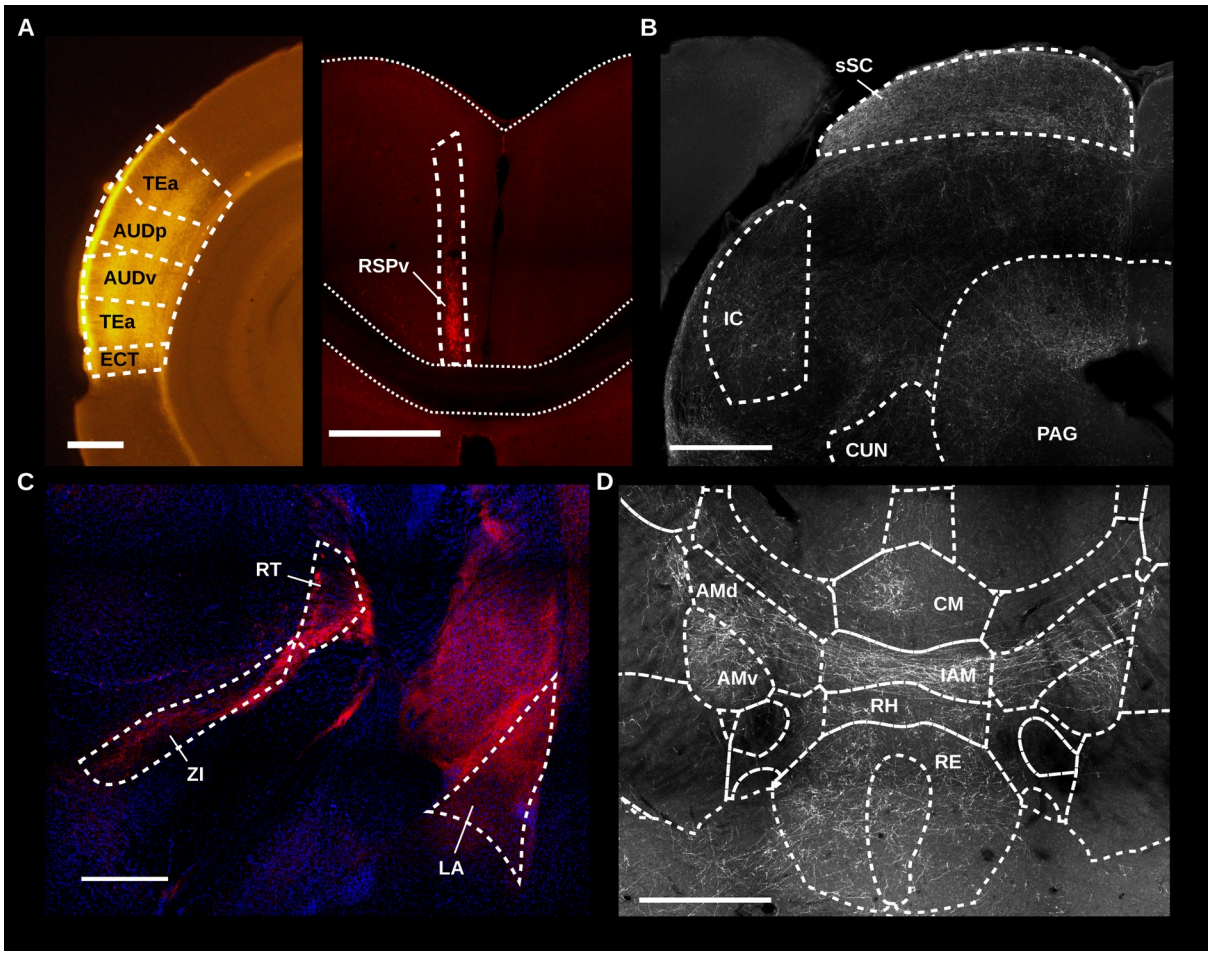

FIGURE S6 | Examination of m-Cherry expression in axon terminals of mouse expressing AAV-hM4D (n=1) suggests various PPnT targets. A. Cortical targets: TEa temporal association area, AUDp posterior auditory area, AUDv ventral auditory area, ECT ectorhinal cortex, RSPv ventral retrosplenial cortex. **B.** Midbrain targets: sSC superficial superior colliculus, IC inferior colliculus, PAG periaqueductal gray, CUN cuneiform nucleus. **C.** Limbic system targets: ZI zona incerta, RT reticular nucleus of thalamus, LA lateral amygdalar complex. **D.** Thalamic targets: CM central medial n., IAM interanteromedial nucleus, RH rhomboid nucleus, RE reuniens nucleus, AMd anteromedial nucleus dorsal part, AMv anteromedial nucleus ventral part. Scale bar, 500 μm.